Equivalent Spring and Damper for Conceptual Suspension Modeling

Siau, G.R.

Award date:
2008

aug. 2008. Siau

Equivalent Spring and Damper for Conceptual Suspension Modeling

ing. G.R. Siau

DCT 2008.091

Master's thesis

Coach(es): dr.ir. I.J.M. Besselink
dr.ir. I. Lopez

Supervisor: prof.dr. H. Nijmeijer

Eindhoven University of Technology
Department of Mechanical Engineering
Section Dynamics and Control

Eindhoven, August, 2008

Samenvatting

Het gebruik van multi-body software resulteert in complexere en nauwkeurige voertuigmodellen. De complexiteit brengt echter een ongewenste verhoging van de CPU tijd met zich mee die nodig is om een simulatie te voltooien. Complexe modellen hebben snelle computers nodig en de behoefte aan modellen die toepasbaar zijn in een real-time omgeving stijgt.

Het doel van deze scriptie is *het begrijpen van de kinematisch en dynamisch gedrag van een wielophanging.* Het tweede doel is *het creëren van een model van een wielophanging dat toepasbaar is in een real-time omgeving.*

Hiertoe is een twee dimensionale beschrijving ontwikkeld van de verticale of equivalente stijfheid van een trailing arm wielophanging. Deze equivalente stijfheid is bevindt zich boven het midden van het wiel en is genaamd *De geometrische Equivalente Stijfheid.* Hiervoor zijn niet-lineaire stijfheid definities gebruikt. Deze niet-lineaire benadering maakt het mogelijk om de beschrijving toe te passen bij grote verticale verplaatsingen van het wiel. De Matschinsky methode is uitgebreid met een definitie van de equivalente voorspanning en een vergelijking is gemaakt met de geometrische equivalente stijfheid. Hieruit blijkt de methode van Matschinsky en de methode van de geometrische equivalente stijfheid uitkomen op dezelfde vergelijking. Beide beschrijvingen zijn extreem nauwkeurig en toepasbaar voor lineaire en niet-lineaire veren alsmede voor grote hoek verdraaiingen van de wielophanging.

Beide beschrijvingen bevatten veel complexe berekeningen en een alternatieve relatie voor de equivalente stijfheid is ontwikkeld. Deze *Gemodificeerde Installatie Ratio* is praktisch aantrekkelijker dan de geometrische of de Matschinsky methode. De gemodificeerde installatie ratio maakt gebruik van lineaire stijfheid definities van de veer. De ratio is toepasbaar voor grote verticale verplaatsingen van het wiel en is extreem nauwkeurig voor lineaire veren. Alle methoden zijn toepasbaar in de conceptuele ontwerpfase van een wielophanging.

Een conceptueel model is gecreëerd inclusief een verbinding tussen wiel en chassis die de fysieke wielophanging vervangt. Daarnaast is een resulterende kracht in de verbinding geïmplementeerd die het effect van een rem koppel op de ophanging modelleert. Om de equivalente stijfheid en de resulterende kracht te testen en te vergelijken met andere methoden, zijn twee multi-body modellen ontwikkeld met behulp van SimMechanics. Deze modellen zijn een referentie model inclusief de trailing arm en een conceptueel model inclusief de verbinding die de fysieke wielophanging vervangt.

De resultaten tonen aan dat het conceptueel model een verlaging van de CPU tijd heeft van $81 - 86\%$. Verder is de CPU tijd van het conceptueel model slechts de helft van de simulatie tijd. Dit bewijst dat het conceptueel model toepasbaar is in een real-time omgeving. Uit de rem test blijkt dat het conceptueel model het anti rise effect niet accuraat modelleert. Het model is dus nog niet voor rem situaties bruikbaar.

Summary

The use of multi-body software results in more complex and accurate vehicle models. The complexity however brings an unwanted increase in CPU time needed to complete a simulation. Complex models need more powerful computers and the need for real-time applicable models is increasing.

In this master thesis the objective is *to understand the kinematic behaviour of a vehicle suspension.* Furthermore, the objective is *to create a suspension model which is applicable in a real-time environment.*

To this end, a two dimensional description of the vertical or equivalent stiffness of the suspension is developed which is called *The Geometric Equivalent stiffness.* For this, nonlinear stiffness definitions are used and this nonlinear approach also enables the relation to be used for larger vertical deflections of the wheel. The Matschinsky method is extended to include pre-deflection and a comparison is made with the geometric equivalent stiffness. It appears that the Matschinsky method and the geometric equivalent stiffness method result in the same equation. Both descriptions are extremely accurate and applicable for linear and nonlinear springs as well as for large angular deflections.

Both relations include a lot of complex calculations and an alternative relation for the equivalent stiffness is developed. This *Modified Installation Ratio* is practically more appealing than the geometric and Matschinsky method. The modified installation ratio makes use of linear stiffness definitions of the spring. The ratio is applicable for large vertical wheel displacements and is extremely accurate for only linear springs. The methods are all applicable for conceptual design of a suspension.

A conceptual suspension model is developed including a joint connection that replaces the physical trailing arm suspension. Furthermore, a resulting vertical force is implemented in the joint that models the effect of a brake torque upon the suspension. To test and compare the equivalent stiffness and the resulting force with other methodes, two multi-body models are developed within SimMechanics. A reference suspension model including the physical trailing arm and a conceptual suspension model including the joint. Results show that the conceptual suspension model has an $81 - 86\%$ decrease in CPU time. In addition, the CPU time is almost half the simulation time which makes the conceptual suspension model applicable for real-time applications. The brake test results show that the joint does not model the anti-rise effect accurate enough. Therefore, the model is nog applicable yet for brake situations.

Contents

Nomenclature

α	Angle between trailing arm and spring axis
$\bar{N}$	Vector perpendicular to a plane
$\bar{V}$	Any vector within a plane
δ	Steering angle
γ	Camber angle
ω	Angular velocity
R	Ratio of parallel sides of two uniform angles
θ	Angular deflection of the trailing arm
θ_A	Angular displacement of the lower A-arm
θ_{nf}	Initial initial angular displacement of the trailing arm
θ_s	Angle between the normal of the lower arm and the spring axis
θ_t	Total angular displacement of the trailing arm
θ_W	Angle between F_{FA} and $F_{perp,W}$
$\triangle F_z$	Vertical force as a result of the load transfer during braking
$\triangle$	Perpendicular length lower A-arm or trailing arm end after angular displacement
$\triangle_E$	Perpendicular length lower spring mount after angular displacement
$\triangle_e$	Perpendicular length with respect to trailing arm at lower spring mount
$\triangle_W$	Perpendicular length tyre contact patch after angular displacement
a	Horizontal distance from suspension pivot point to wheel center
A_{12}	Orientation matrix chassis to wheel carrier
b	Perpendicular distance from suspension pivot point to spring axis
c	Length suspension pivot point to upper spring mount
c_A	Perpendicular stiffness at lower A-arm end
c_{FA}	Stiffness equivalent spring
c_F	Stiffness physical spring

c_k	Position vector knuckle frame to center of gravity of knuckle
c_{perp}	Perpendicular stiffness at trailing arm end
c_W	Perpendicular stiffness at tyre contact patch
d	Horizontal length suspension pivot point to upper spring mount
d_1	Position vector chassis frame to lower arm frame
d_2	Position vector lower arm frame to knuckle frame
d_3	Position vector lower arm frame to top damper mount
d_c	Position vector ground frame to chassis frame
e	Vertical length suspension pivot point to upper spring mount
f	Displacement of the physical spring
f_0	Pre-deflection of physical spring
F_b	Brake force
F_{DA}	Equivalent vertical damper force
F_D	Force of the physical damper
F_{F0}	Pre-load of physical spring
F_{FA0}	Pre-load of equivalent spring
F_{FA}	Equivalent vertical spring force
F'_{FA}	Vertical force at wheel center after initial displacement
F_F	Force of the physical spring
$F_{perp,A}$	Force acting perpendicular with respect to the lower A-arm
$F_{perp,W}$	Perpendicular force at tyre contact patch
F_{perp}	Force acting perpendicular with respect to the trailing arm
F_{zb}	Vertical force as a result of braking
F_z	Sprung wheel force
g	Length trailing arm pivot point to lower spring mount
i_D	Damper ratio
i'_D	Damper ratio after initial displacement
I_{Fs}	Standard installation ratio
i_F	Spring ratio
i_R	Modified installation ratio
i_r	Installation Ratio
i'_R	Modified installation ratio after initial displacement
k_{DA}	Damping equivalent damper

k_D	Damping physical damper
L	Trailing arm length
l^c	Kingpin axis
l_0	Spring length at $\theta = 0$
L_{AD}	Length line of intersection to end of lower A-arm
L_{BC}	Length lower spring mount to pivot point lower A-arm
L_{BD}	Length of the lower A-arm
l_n	Natural or unloaded spring length
l_s	Spring length
L_W	Length line of intersection to tyre contact patch
n	Perpendicular distance from wheel center to trailing arm reference position
p	Brake torque distribution
r_{12}	Position vector chassis to wheel carrier
r_k	Position vector ground to knuckle
s	Vertical wheel displacement
s'	Vertical displacement wheel center after initial displacement
s_0	Pre-deflection of equivalent spring
t	Time
T_b	Brake torque
V	Forward velocity of the vehicle
v_{AZ}	Vertical velocity at the center of the tyre contact patch
v_A	Velocity magnitude of the tyre contact point
v_a	Velocity increase in line with distance a
v_B	Perpendicular velocity lower spring mount with respect to trailing arm
v_b	Velocity increase in line with distance b
v_D	Velocity of damper piston
v_d	Velocity lower spring mount perpendicular to spring axis
v_f	Velocity lower spring mount in line with spring axis
v_{MZ}	Vertical velocity wheel center
v_M	Velocity magnitude wheel center
z_E	State variable for elastic compliance
z_G	State variable for the motion degrees of the macro joint
z_K	State variables for bump and rebound plus steering

Chapter 1

Introduction

1.1 Problem Statement

Multi-body software enables the engineer to create a realistic model of a vehicle. Complete suspension links and chassis components can be modeled with accurate mass and inertia properties that agree with the physical properties of the particular components of the vehicle. This vehicle model eventually contains a large number of bodies that represent the various suspension and chassis components. This results in a complex set of differential algebraic equations (DAE) that has to be solved each time step which consumes a lot of time and CPU capacity. These full vehicle multi-body models are very effective and convenient when investigating the exact kinematics and static behaviour of a vehicle suspension for example. Dynamic behaviour investigations however will consume much more simulation time or require expensive high performance computers. Generally this does not give major problems except when the multi-body model is applied in a real-time environment.

An ideal model in the process of vehicle development and research would be a vehicle model that is fast enough for real-time applications such as a driving simulator or a model that is applicable in HIL (Hardware In the Loop) environments. HIL applications are used to evaluate and validate vehicle components during the development process. Rather than testing these components with a vehicle prototype, HIL allows the testing of new components and prototypes while communicating with software models that simulate the remaining part of the vehicle system. The physical components being tested respond to the simulated signals as though they were operating in a real vehicle. To replace the time consuming multi-body approach different techniques have been developed, e.g. conceptual suspension models. In publications about these software tools a general overview of the conceptual design procedures is given, but the exact method is never described because of commercial reasons.

Within the Technical University of Eindhoven a group of students, called the University Racing team Eindhoven (URE), designs and creates a small racing car that will compete with other racing car creations throughout Europe. A full multi-body model of the racing car already exists but a need for a real-time vehicle model also emerges within this group. A real time model that can be used in a driving simulator enabling the students to virtually drive a predetermined track that is used in the competition. This will give some insight in the handling of the race car and helps to train the driver. A first step in developing a real time vehicle model is to understand what actually happens with a suspension before creating a complete vehicle model. The next step is to create a methodology that results in a conceptual suspension model.

1.2 Goals

The objectives of this thesis are:

- *To understand the kinematic and dynamic behavior of a vehicle suspension*
- *To create a suspension model which is suitable for real-time simulations*

Knowing how and which forces act upon the suspension will give a better understanding of the suspension kinematics and dynamics and will give a good insight in how to implement them into the real-time model. A literature study will be made to see what kind of methods already exist.

With these objectives in mind a simple two dimensional suspension model is used since it allows a clear view on the suspension kinematics and dynamics. The vehicle model includes a basic trailing arm suspension with a spring and damper combination. Obviously, some features are excluded, namely steering and suspension compliance. A feature as compliance however plays an important role in suspension analysis and will be explained further on in the report. The vehicle model will contain the dimensions and mass properties of the formula racing car.

1.3 Outline of the Report

Chapter 2 contains a literature study including general background information of suspension modeling and the challenges that come with it. The chapter also includes an overview of the different techniques that already have been developed, as well as an overview of the software available to the industry to create a conceptual suspension model. The chapter ends with a comparison of the techniques found in literature.

Chapter 3 covers the equivalent stiffness and damping of springs and dampers. These equivalences are the main parts of the methodology to create a conceptual suspension model and basically includes the kinematic characteristics of the suspension. This chapter also discusses a new technique that has been developed and is applicable for any angular deflection of the trailing arm. This technique includes a ratio that is called the 'Modified Installation Ratio' and the derivation of this ratio assumes the implementation of a linear spring characteristic.

A model of a trailing arm suspension is designed as a reference to compare it to the conceptual model. Chapter 4 discusses the multi-body models of the reference and conceptual suspension that are created with SimMechanics. This is the multi-body toolbox within MATLAB/Simulink. Further topics are the definition of the wheel trajectory, connection of the spring and damper with the vehicle body, etc. The chapter ends with the behaviour of the suspension during braking and how the brake system is implemented in the conceptual suspension model.

Different approaches exist to obtain the equivalent spring and damper rate. Hence, a comparison with two of these other approaches will be made to illustrate the differences in results. Chapter 5 discusses and evaluates the test results of the comparison. A kinematic simulation is performed where the vehicle model is fixed in space and is subjected to a large amount of vertical wheel deflection. Furthermore, the kinematic tests are performed for a linear and a nonlinear spring. A dynamic simulation is performed where the vehicle model will travel with a constant velocity after which it will be subjected to a brake torque. All simulation tests are performed on a computer with an Intel 1.4 GHz processor and 512 internal RAM memory. Computations and modeling are performed using MATLAB version 2000*a*.

Finally chapter 6 covers the conclusions of this thesis and the recommendations for further development and application of the method of conceptual suspension modeling.

Chapter 2

Overview of Conceptual Suspension Modeling Techniques

2.1 Background Information on Suspension Modeling

In the automotive sector plenty of research has already been done to improve vehicle suspensions. Every type of vehicle has its own list of demands to which the suspension must comply. One can think of saloon vehicles where comfort is emphasized or racing cars where vehicle handling is emphasized in comparison to comfort. In general, a compromise is made between the two in order to increase the drivability of the car for every day use. Besides the technological aspect of suspension development there is also a financial aspect. There is a balance between suspension improvement and the costs to make these improvements happen. Cars developed for every day use are designed by focussing more on the low production costs of the suspension. Racing teams on the other hand have a larger budget that enables the engineers to implement more improvements to their racing car. In order to find a better compromise between handling, comfort and costs causes the future vehicle suspensions to become more and more complex. Technical knowledge from several aspects is required in order to develop and improve vehicle suspensions. An example of a modern front suspension is shown in figure 2.1.

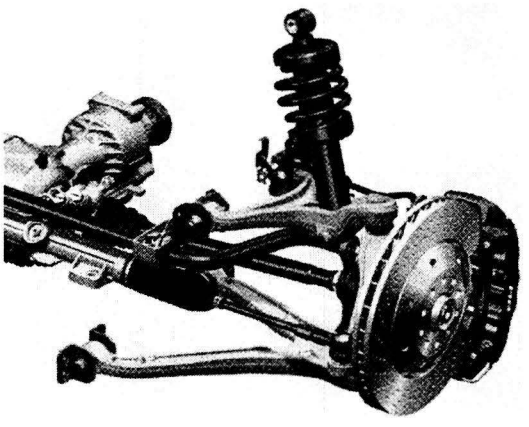

Figure 2.1: Front suspension of the Audi R8 [1]

One of the important aspects is the suspension kinematics. The suspension kinematics can be interpreted as the relative movement of the wheel with respect to the chassis. The connections between the wheel and the chassis prescribes the trajectory of the wheel in the three dimensional space. For an independent suspension for example, the position and orientation of the control arms prescribe the motion of the wheel relative to the vehicle body in a unique trajectory. As an example, the front view of an independent suspension is illustrated in figure 2.2.

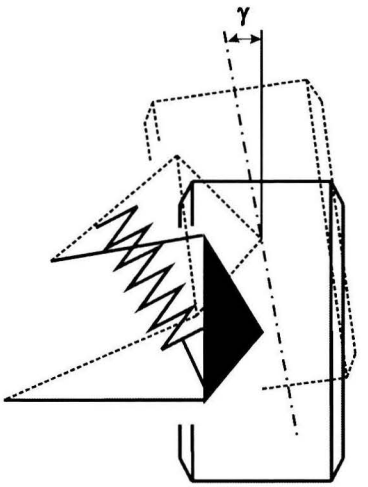

Figure 2.2: Example of a local position and orientation change of the wheel

It is clear to see that the orientation of the wheel changes with bump. This orientation γ that is illustrated in the figure is known as the camber angle. During the vertical movement the wheel may also encounter changes in other orientations as toe and caster as well as changes in longitudinal and lateral position. More about wheel positioning and orientation can be found in [2], [3], [4] and [5].

However, every material will deflect under load. The question then emerges of how unique this trajectory really is. This brings us to another important aspect: suspension compliance. Every part that is under load will deflect and this deflection can modify the suspension kinematics significantly. The modification of the suspension geometry that occurs while under load is called suspension compliance. Compliance is caused in different ways: rubber suspension bushings, rubber mounted steering racks and steering joints, hard parts that deflect under load, etc. For racing applications, generally one wants as little compliance as possible. For normal road car applications a certain degree of compliance is required to achieve good ride comfort. It may even be used to achieve the desired handling characteristics.

Another technical aspect is the stiffness and damping of the suspension. The choice of the stiffness of the spring, is dependent on the permissible amount of pitch, roll, etc that the engineer has determined before. Pitch, roll and yaw effects of the vehicle can be seen in figure 2.3. During the design process of the suspension the engineer will compute a wheel rate which defines the vertical stiffness of the suspension. The wheel rate is defined as the vertical force per unit vertical displacement of the wheel center relative to the vehicle body. Using this wheel rate and the suspension kinematics the engineer can calculate the stiffness of the spring.

2.2 Literature on Conceptual Suspension Modeling

Within the automotive industry there are simulation software developers and car manufacturers that already have investigated conceptual suspension models. The information that has been found concerning these models is presented in this chapter.

2.2.1 The Lotus Simulation and Analysis Model

Lotus uses a model which replaces the physical items with simplified equivalents [6]. The resulting model consists of 5 sub-models, the vehicle body, two independent rear suspension models and two independent front suspension models including the steering system. The vehicle body is assumed to be rigid with six degrees of freedom. In figure 2.3 an example of the body and its degrees of freedom is shown.

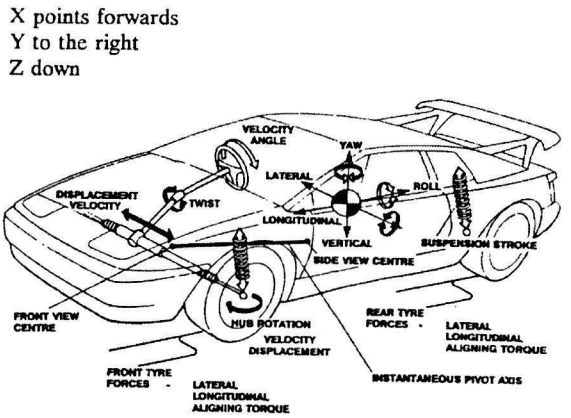

Figure 2.3: Lotus vehicle body and its degrees of freedom [6]

The suspension modeled represents an independent suspension system. The assumption made by Lotus is that the wheel hub has only one degree of freedom for wheel travel and rotates about a pivot axis that is fixed to the vehicle body. The suspension is idealized by considering it as a single swing arm attached to the body at the pivot axis. This representation of the front suspension is shown in figure 2.4.

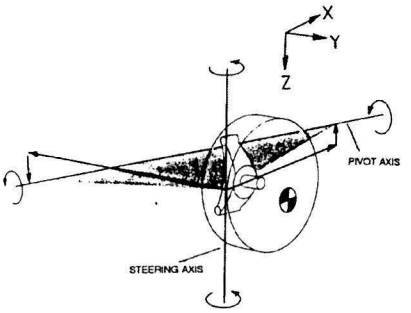

Figure 2.4: Front suspension [6]

The front suspension uses the same concepts as the rear suspension but adds a steering axis to the model. This steering axis is attached to the effective swing arm as can be seen in figure 2.4. This model is equipped with a spring/damper model which is attached to the swing arm together with the tyre model. The spring stiffness is chosen to be constant while the damping characteristic is taken from a look-up table (force versus velocity). In theory, knowledge of the pivot axis allows the calculation of the coordinates of the wheel hub. However, the suspension data is calculated 'off-line'. It is preferable to define additional suspension data in look-up tables which are all defined as a function of bump. The bump is defined as the displacement of the wheel center in vertical direction. Examples of data are: Toe angle, Camber angle, damper piston displacement, etc.

The significant development by Lotus is the generic approach to modeling the suspension by means of using a pivot axis. With this simplicity comes the added advantage of using suspension data directly from suspension test rigs and thus reducing the need for detailed design data. This method is also applicable in the initial design stage where mostly suspension data is available in the form of geometry. However, no information is available about how the spring stiffness or damping characteristic are determined whereas the understanding of the suspension behaviour is one of the main objectives.

2.2.2 The Suspension Composite Joint

Within the Automotive Institute of Technology (KATECH) and the Advanced Institute of Science and Technology (KAIST), both situated in Korea, a suspension modeling method is developed for real-time dynamic simulation [7]. This method includes Suspension Composite Joints to model the vehicle suspension. Basically, the model consists of a vehicle body with four composite joints that represent the suspension on each side of the vehicle. A multi-body approach is used to obtain the kinematics of the suspension and the composite joints as well as the orientation of all the bodies with respect to the ground. An example of a suspension is the MacPherson strut. A schematic suspension diagram of the MacPherson strut is shown in figure 2.5.

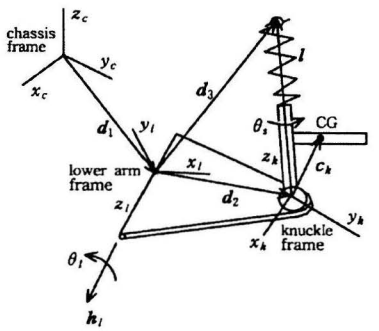

Figure 2.5: MacPherson strut suspension diagram [7]

Common multi-body modeling methods will encourage the engineer to model the lower arm and the upper piston as rigid bodies. The composite suspension joint however models these components as massless links. Combining these massless links with other suspension members modeled as rigid bodies will reduce the amount of bodies which results in a decrease in equations of motion and constraint equations.

The kinematic characteristics of the composite joint are derived using the transformation matrix of the knuckle frame with respect to the chassis. A transformation matrix defines how to map points from one coordinate space into another coordinate space using Euler angles for example. Euler angles

define an angular rotation sequence to obtain the orientation of a body. First the body rotates about the local z axis, then the local x axis and finally the local z axis. The knuckle frame can be defined by these $z-x-z$ Euler angle (ϕ, θ, θ_s) rotations from the chassis. After the first two rotation angles, the axis l^c coincides with the z axis of the rotated frame. The final rotation angle is the steering motion about l^c. This axis is also called the kingpin axis. Thus if the vector of the kingpin axis is known the remaining rotation angles ϕ and θ can be determined. The vector of the kingpin can then be written as

$$l^c = ({l_x}^c, {l_y}^c, {l_z}^c) = {d_3}^c - {d_2}^c \tag{2.1}$$

where the superscript c represents the vectors in the chassis frame. The equations for the angles ϕ and θ are derived using this equation together with the rotation matrix. Differentiations with respect to time are then used to obtain the velocity of the kingpin axis and the angular velocity and accelerations of ϕ and θ. The knuckle frame is defined by successive rotations of the chassis frame and the angular velocity of the knuckle must be defined with respect to the ground. The vector from the ground to the center of gravity of the knuckle r_k can be written as

$$r_k = d_c + d_1 + d_2 + c_k \tag{2.2}$$

where d_c is the vector from the ground to the chassis frame. The velocity and acceleration can then be derived by differentiations with respect to time. The general matrix form for a set of equations of motion can then be obtained including q, $\dot{q}$ and $\ddot{q}$ representing the position, velocity and acceleration of the system. These set of equations of motion are then implemented in a simulation program.

So no simplification of the suspension in the form of a pivot axis is used, but a full multi-body approach with massless links. This method could be used in the conceptual design stage, because of the availability of the suspension's geometry that is needed in order to perform the multi-body analyses. However, this suspension composite joint does not include a force analyses that gives more insight in the behaviour of the suspension. The manner in which the spring stiffness is determined is not discussed in [7].

2.2.3 The Macro Joint

This method that has been developed by A. Eichberger and W. Rulka [8] employs a so called macro joint to model the suspension of a vehicle. The joint approach is based on reduction steps. These steps convert a complex full multi-body suspension model into a conceptual suspension model containing the relevant kinematics. The graphical representation of the macro joint is given in figure 2.6.

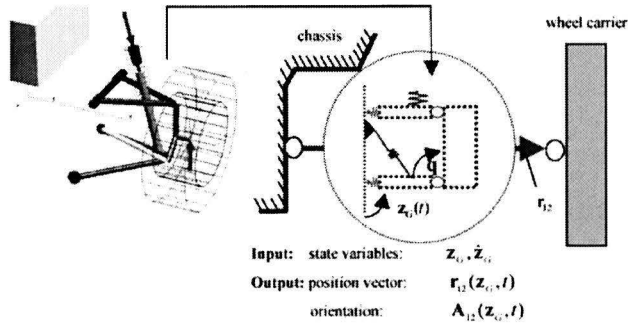

Figure 2.6: Input and output of the macro joint [8]

In a first step the flexibility of the bodies is being neglected and idealised joints replace the bushings in the model. This results in a model without compliance and therefore creating a pure kinematic suspension model including rigid bodies. Next, the dynamic effects of the bodies with small masses are neglected. The macro joint describes the kinematic bump and rebound behaviour by using relative coordinate multi-body systems formalisms as position vectors and rotation matrices. The relative position r_{12} and the relative orientation A_{12} are a function of the motion degrees z_G of the joints. The equations of motion are derived by partitioning the kinematic variables into independent state variables, such as z_G, and dependent variables q of the suspension rods.

Suspension compliance can also be modeled by the macro joint approach. Two kinds of compliance modeling are possible. Individual stiffness properties of the suspension bushings for example can be modeled by adding the appropriate state variables. Overall suspension compliance can be modeled by separating the relative movement of the wheel with respect to the chassis into a kinematic part and a elastic part of the wheel hub as is shown in figure 2.7.

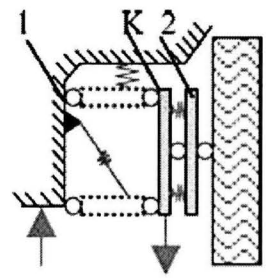

Figure 2.7: Overall compliance modeling [8]

The additional deformation degrees of freedom increases the system size because of the increase of state variables. However, this has little to no influence on the CPU performance.

The next reduction step includes the assumption that high frequency dynamics are not relevant for typical handling simulations. The corresponding quasi-static effects however must be taken into account. During this second reduction step the motion equations of the wheel carrier are partitioned into state variables z_K for bump and rebound plus steering and z_E for the elastic compliance.

$$\ddot{z}_K = h_K(\dot{z}_K, z_K, \dot{z}_E, z_E, t) \tag{2.3}$$
$$\ddot{z}_E = h_E(\dot{z}_K, z_K, \dot{z}_E, z_E, t) \tag{2.4}$$

The assumption that only the quasi-static solution is relevant, thus $\ddot{z}_E = 0$ and $\dot{z}_E = 0$, results in a static equation for the differential equation of elastic deformations:

$$\ddot{z}_K = h_K(\dot{z}_K, z_K, 0, z_E, t) \tag{2.5}$$
$$0 \quad = h_E(\dot{z}_K, z_K, 0, z_E, t) \tag{2.6}$$

The resulting set of DAE is solved by a DAE solver for off-line simulation. The macro joint approach shows some similarities with the composite joint approach. Neglecting smaller masses with respect to larger masses for instance. The macro joint however takes the reduction of a model even further and more effectively by taking out the effects due to high frequency dynamics. However, the similarities also causes the model to inherit the disadvantages.

2.2.4 The Matschinsky Model

To accurately model the dynamic behaviour of vehicles it is important to capture the suspension kinematics. Commercial software commonly models all the suspension links. However, it is still useful and insightful to find other approaches. To this end, the force/deflection characteristics of the wheel center relative to the vehicle body is estimated. This is also known as the wheel rate which is discussed in paragraph 2.1. This wheel rate is dependent on the geometry of the suspension and also of the orientation and stiffness of the actual suspension spring. Hence, a relation must exist between the wheel rate and the spring stiffness. Wolfgang Matschinsky [2] derives a so called 'reduced spring rate' and a 'reduced damper rate'. The reduced spring rate is the derivative of the sprung wheel load F_{FA} with respect to the vertical wheel displacement s (See figure 2.8). It is also the same as the wheel rate. The 'reduced damper rate' is the quotient of the vertical force F_{DA} resulting from the damper and the vertical wheel velocity v_{AZ}. Matschinsky computes the derivatives and quotients analytically.

Reduced spring rate

The 'spring ratio' is the quotient of the sprung wheel force F_{FA} and the force of the spring F_F. A simple example of an independent suspension is given in figure 2.8.

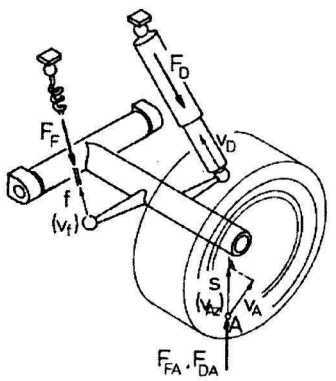

Figure 2.8: Independent 'swing axle' suspension [2]

Here, v_f is the velocity along the axis of the spring and v_{AZ} is the vertical velocity at the center of the tyre contact patch. The power exerted by F_{FA} and v_{AZ} must be balanced by the power of F_F and v_f. The power balance resulting from the damper force will be discussed in the next paragraph. This balance of power results in a relation for the spring ratio i_F:

$$i_F = \frac{v_f}{v_{AZ}} = \frac{F_{FA}}{F_F} \tag{2.7}$$

Figure 2.8 shows the velocity v_A which is the velocity of the tyre contact point. The direction of this velocity and thus the vertical component v_{AZ} together with the inclination of the spring will change with vertical wheel displacement. This will result in a variable spring ratio. The 'spring stiffness' is the quotient of the change in spring force (dF_F) and the change in elongation of the spring (df) which may be variable.

$$c_F = \frac{dF_F}{df} \tag{2.8}$$

The 'reduced' spring stiffness is the quotient of the change in sprung wheel force F_{FA} and the change in vertical wheel displacement s.

$$c_{FA} = \frac{dF_{FA}}{ds} \tag{2.9}$$

The sprung wheel force F_{FA} is a function of the spring force F_F and the spring ratio i_F as can be seen in (2.7). Rewriting the derivative results in a general expression for the reduced spring rate:

$$c_{FA} = c_F {i_F}^2 + F_F(\frac{di_F}{ds}) \tag{2.10}$$

The first term of the of equation (2.10) is well known and used in the industry. The second term of the equation is the so called 'kinematic spring rate'. This second term includes the change in spring ratio with respect to the change in vertical displacement of the wheel. The term can be imagined for a spring of constant length, and thus only producing a preload force and no stiffness, rotating about its pivot point. The spring ratio changes when the spring mount shifts along the suspension link for example. A geometrical representation of the spring ratio will be discussed next. Figure 2.9 shows a simple trailing arm suspension including a spring. In this case F_z is the sprung wheel force and

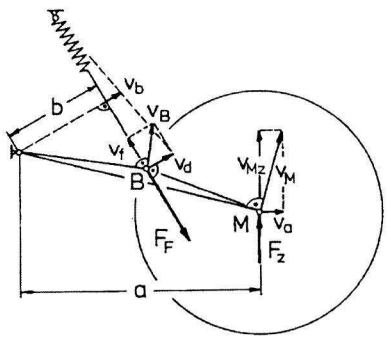

Figure 2.9: Kinematic influence on the reduced spring stiffness [2]

F_F is the spring force. Taking the balance of moments results in the spring ratio of the trailing arm suspension $i_F = b/a$. The second term of (2.10) can now be derived.

$$\frac{di_F}{ds} = (\frac{\partial i_F}{\partial a})(\frac{da}{ds}) + (\frac{\partial i_F}{\partial b})(\frac{db}{ds}) \tag{2.11}$$

The derivatives da/ds and db/ds can be determined graphically using figure 2.9. The vertical component v_{MZ} of the wheel center velocity v_M equals to the vertical velocity of the wheel v_{AZ}. The radius a is increased bij the horizontal component v_a. This gives $da/ds = v_a/v_{MZ}$.

From v_M the velocity v_B of the lower spring mount can be derived. The component v_f is the velocity of the spring elongation and the component v_d is perpendicular to the spring. The latter component increases the radius b by velocity v_b. This gives $db/ds = v_b/v_{MZ}$. This results in the final expression for the reduced spring rate.

$$c_{FA} = c_F \left(\frac{b}{a}\right)^2 + F_F \left[-\left(\frac{b}{a^2}\right)\left(\frac{v_a}{v_{MZ}}\right) + \left(\frac{1}{a}\right)\left(\frac{v_b}{v_{MZ}}\right)\right] \tag{2.12}$$

Reduced damper rate

The damper of figure 2.8 is subjected to the same conditions as the spring. However, the damper force F_D is not dependent on the piston travel but on the piston velocity v_D.

$$F_D = k_D v_D \tag{2.13}$$

The balance of power between the damper force and velocity with the vertical force F_{DA} and vertical velocity v_{MZ} at point A at the tyre contact patch results in a relation for the so called 'damper ratio' i_D.

$$i_D = \frac{v_D}{v_{MZ}} = \frac{F_{DA}}{F_D} \tag{2.14}$$

The 'reduced damper rate' can be written as:

$$k_{DA} = \frac{F_{DA}}{v_{MZ}} \tag{2.15}$$

Substituting (2.14) and (2.13) into (2.15) results in the final expression for the reduced damper rate.

$$k_{DA} = k_D {i_D}^2 \tag{2.16}$$

The damper rate represents the instantaneous relationship of the damper velocity and force. The method of Matschinsky gives a detailed force analysis that results in an insightful relation between the spring stiffness and the wheel rate. The use of velocity components makes this method not suitable for conceptual design. Calculating da/ds and db/ds is a mathematical challenge because b is not directly a function of s, but is certainly not an impossible one. Furthermore, there is no clear explanation of how preload is implemented. Also, no method is available about implementing suspension behaviour during braking for example.

2.2.5 Three Dimensional Installation Ratio for a Dual A-Arm Suspension

A different approach of obtaining the relation between the wheel rate and the stiffness of the suspension spring is presented by E. Manes and J. Starkey [9]. This relation includes the so called 'installation ratio'. The installation ratio relates the vertical motion of the tyre contact patch with the motion of the suspension spring. The innovation of E. Manes and J. Starkey is the three dimensional calculation of the ratio which is applied to a double A-arm suspension.

The derivation starts with defining planes of the lower and upper A-arms by using a vector analysis. The upper and lower planes are defined by two vectors contained within the upper and lower A-arm. These planes of the A-arms will intersect at a line in space. The plane normals N_U and N_L of these A-arms are created by taking the cross product of the plane vectors. Now the vector equation can be used:

$$\bar{N} \cdot \bar{V} = 0 \tag{2.17}$$

where $\bar{N}$ represents the vector perpendicular to a plane and $\bar{V}$ any vector within that plane. Taking the cross product of the plane normals results in a vector that is parallel to the line of intersection. A third plane can then be defined that determines the distance from the line of intersection to the contact patch of the tyre as is shown in figure 2.10.

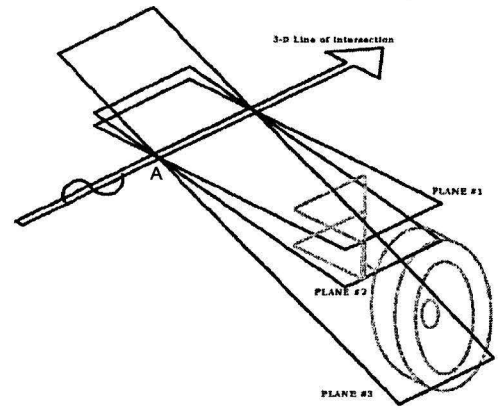

Figure 2.10: Planes from line of intersection to contact patch [9]

Figure 2.11 shows the view of the lower A-arm including the applied forces where A equals the position of the line of intersection and B equals the position of the where the lower A-arm rotates about. The analysis uses basic geometry and balance of moments about point B to relate the spring force F_F with the force acting perpendicular to the lower A-arm $F_{perp,A}$:

$$F_F = F_{perpA} \frac{L_{BD}}{L_{BC} \cos\theta_S} \tag{2.18}$$

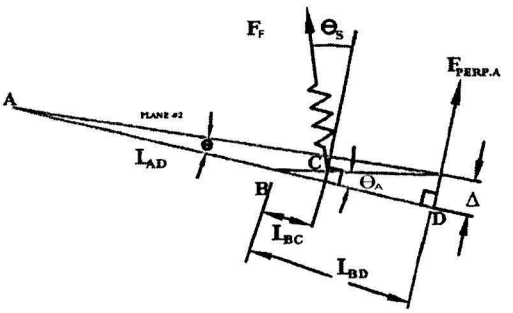

Figure 2.11: View of lower A-arm along the line of intersection [9]

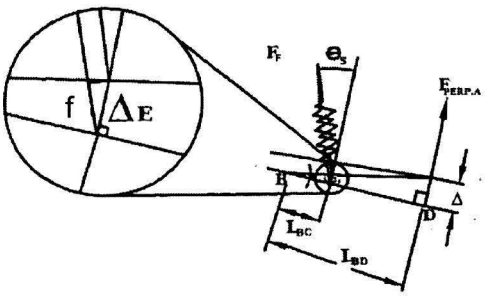

Figure 2.12: Assumption for the spring elongation [9]

Figure 2.12 shows a detailed view of the lower A-arm after a small rotation of θ_A about rotation point B where f equals the spring elongation. The assumption is made that the spring elongation is related to the distance $\triangle_E$ by $f = \triangle_E \cos\theta_S$. A relation is then found between the perpendicular distance $\triangle$ and $\triangle_E$:

$$\tan\theta_A = \frac{\triangle_E}{L_{BC}} = \frac{\triangle}{L_{BD}} \tag{2.19}$$

This equation can be used to derive the relation for the spring elongation f.

$$f = \frac{L_{BC}\cos\theta_S\triangle}{L_{BD}} \tag{2.20}$$

Assuming small angular deflections the linear rates c_A and c_F become:

$$c_A = \frac{F_{perp,A}}{\triangle} \tag{2.21}$$

$$c_F = \frac{F_F}{f} \tag{2.22}$$

Relations (2.20) and (2.18) can be used to solve the linear rate c_A at the point where $F_{perp,A}$ is applied. This rate is also a function of the linear spring stiffness.

$$c_A = c_F\left(\frac{L_{BC}}{L_{BD}}\right)^2(\cos\theta_S)^2 \tag{2.23}$$

The equation above relates the actual spring stiffness c_F to an equivalent spring rate c_A positioned at point D. The next step is to relate this equivalent spring rate to the effective spring rate c_W present at the tyre. Figure 2.13 shows the view of the planar model along the line of intersection where F_{FA} equals the vertical force and s equals the vertical wheel displacement. Noting that $c_W = F_{perp,W}/\triangle_W$ and reminding $c_A = F_{perp,A}/\triangle$, the balance of moments $F_{perp,A}L_{AD} = F_{perp,W}L_W$ can be rewritten.

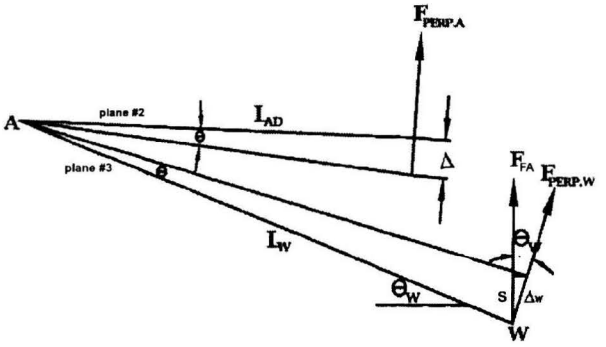

Figure 2.13: View of planar model along the line of intersection [9]

For small angular deflections θ again the tangent function can be used in order to relate the two perpendicular distances $\triangle$ and $\triangle_W$. The relation for c_W can then be written as:

$$c_W = c_F \left(\frac{L_{BC}}{L_{BD}}\right)^2 (\cos\theta_S)^2 \left(\frac{L_{AD}}{L_W}\right)^2 \tag{2.24}$$

The equation (2.24) gives the equivalent spring rate perpendicular to plane #3. A relation must be found for the wheel rate c_{FA} and this relation must be a function of the perpendicular rate c_W. To do so the balance of moments is obtained and simple trigonometry results in a relation for the displacement $s = \triangle_W \cos\theta_W$. The final relation for the wheel rate c_{FA} can then be written as:

$$c_{FA} = c_F \left(\frac{L_{BC}}{L_{BD}}\right)^2 \left(\frac{\cos\theta_S}{\cos\theta_W}\right)^2 \left(\frac{L_{AD}}{L_W}\right)^2 \tag{2.25}$$

The relation above gives the three dimensional wheel rate where the installation ratio equals to:

$$i_r = \frac{L_{BC}\ \cos\theta_S\ L_{AD}}{L_{BD}\ \cos\theta_W\ L_W} \tag{2.26}$$

The vertical force analysis can be used to compute other suspension motions such as camber and three dimensional motion of the contact patch. Also, if a higher i_r is obtained (by manipulating the suspension geometry) a lower spring stiffness can be chosen in order to achieve the desired wheel rate. A lower spring stiffness results in a spring that is smaller and thus lighter in weight. In turn these qualities of the spring tribute to the overall dynamics of the suspension in a positive manner. The disadvantage of the installation ratio is the use of linear stiffness and rates that assume only small angular deflections. Choosing small deflections means that the situation is treated for a damper instead of for a spring. The results are therefore incomplete. The assumptions will also reduce the ratio's appropriateness of implementing a nonlinear spring stiffness. Furthermore, no method is found within this literature about how to implement preload. It is however suitable for conceptual design.

2.3 Conceptual Suspension Models available in Commercial Software

Besides the analytic approaches available in literature, that have been created to obtain an effective suspension model, there is also commercial software available that provides conceptual suspension models and real-time applicable vehicle models.

2.3.1 Suspension Analysis Toolbox (ve-DYNA)

The ve-DYNA Suspension Analysis Toolbox [10] contains a conceptual suspension module. This toolbox uses a fully automated suspension data generation process using a K&C (Kinematics and Compliance) test rig. The test rig uses a real vehicle for test measurements. An other option is to use an ADAMS multi-body vehicle model and test rig. An overview can be seen in figure 2.14.

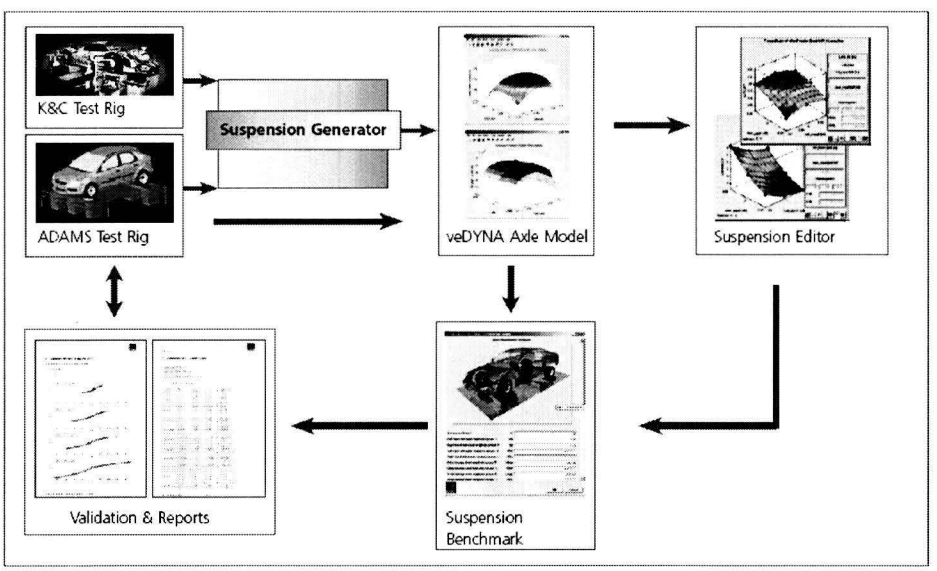

Figure 2.14: veDYNA Suspension Analysis Toolbox [10]

First a Suspension Generator is used to obtain the suspension characteristics. Separate tables of the suspension kinematics and compliance will be generated. In addition spring/damper deflections and anti roll characteristics are computed. These are then implemented in a suspension model containing the characteristics of the suspension.

The second step is the evaluation and validation of the model. This will be done by the Suspension Benchmark which is a virtual test rig that tests the suspension model, reproduces the kinematics and compliance and finally compares the results with the original test results.

Finally, the Suspension Editor enables conceptual suspension studies. The generated suspension model data can be modified by means of a graphical user interface. This results in the possibility to alter certain suspension parameters to study the influence on vehicle handling behaviour.

2.3.2 Virtual Suspension Joint (SIMPACK)

The method that SIMPACK [11] uses is comparable with the method of veDYNA. CAD/MBS (Multi Body System) models are used to obtain geometry data and measurements on a virtual test rig resulting in e.g. suspension data. Then an ODE (Ordinary Differential Equation) model is created of the suspension. To reduce the model, two so called 'joints' are used within SIMPACK.

The 'virtual joint' describes the kinematics of the suspension. These kinematics are described by functions dependent of s and δ: $f_i(s, \delta)$ where s = vertical displacement of the wheel center and δ = steering. Examples of these functions are base (x-position), toe angle, camber angle, etc. These functions can then be used in look-up tables.

The equations of motion of the CAD/MBS model (with model reduction) are automatically generated by SIMPACK and converted into source code. This code can then be used in Simulink for example to be used for real time applications.

The virtual joint uses look-up table based kinematics and elastokinematics that requires a look-up table generator. The 'macro joint' of A. Eichberger and W. Rulka [8], as described in 2.2.3, does not use these look-up tables. This joint uses data input of the kinematic mounting points and also data input of the orientation and properties of the bushings. The macro joint also include the effects due to wheel oscillations and higher frequency vehicle dynamics up to 20 Hz. Both joints are applicable for use in a real-time environment.

2.3.3 Conceptual Suspension Model (ADAMS)

The conceptual suspension module (CSM) [12] is part of the motion simulation software called ADAMS. CSM is also a method of implementing functional suspension characteristics by using predefined trajectories of the wheel hub while subjected to vertical wheel displacement, a steer angle and external forces. The orientation of the wheel hub changes due to the attachment of rubber bushings and other applications causing suspension compliance. Keeping these phenomena in mind, the functional curves can either be kinematic or elastic. The kinematic curves are all a function of the vertical wheel displacement and the rotation of the steering pinion. The curves describing compliance are all a function of the road loads such as longitudinal and lateral forces, brake forces, aligning torque, etc. A subsystem within the CSM module uses so called 'suspension characteristic files' which contain the wheel hub movements with respect to the vehicle body.

To define the wheel hub motions CSM uses two types of joints, a **curve** and **point-to-curve** joint. The curve joint allows one to define an open or closed trajectory in three dimensions which is attached rigidly to any part of the model. The point-to-curve joint keeps the positions of a marker, belonging to a particular part, lying on the given trajectory. The given trajectory emerges from the kinematic curve functions. The joint is a kinematic constraint that removes two translational degrees of freedom and thus leaves four degrees of freedom to the connecting marker of the other part. The conceptual suspension, together with the kinematic and compliant (K+C) suspension characteristics data, provides the modeling functionality of a conventional suspension model but without creating a multi-body suspension model. This is an obvious requirement of conceptual design in general because sufficient data to create suspension prototypes is simply not available. Another requirement of conceptual design is short computation times and thus simplifying the multi-body mode.

2.4 Literature Evaluation

The industry recognizes the need for conceptual suspension design and modeling and thus many different approaches are available. However, the different approaches show a lot of similarities. All of the methods that are discussed use reduction steps in order to create a conceptual suspension model. One general reduction step is the elimination of the mass and inertia properties of the bodies with relative small masses with respect to the larger masses of the sprung masses, wheel hub and wheel mass e.g.

This important step already reduces the amount of constraint equations.

The main differences can be found in the way the trajectory and the change in motion of the wheel (camber change e.g.) is obtained with respect to the vehicle body. Lotus uses an instantaneous pivot axis from which the change of motion e.g. can be derived. The composite joint approach uses pure multi-body analysis including position vectors and orientation matrices whereas the macro joint approach uses state variables to obtain the wheel trajectory, camber change, etc. Commercial software tools generally use look-up tables that contain functional equivalents of the wheel trajectory, camber change, toe change, etc. These functional equivalents are obtained using a physical vehicle or a multi-body vehicle model. These suspension analysis tools are sufficient when investigating an existing suspension or when creating a real time capable vehicle model from this vehicle. However, during prototyping, there is simply not enough data available. On the other hand, ADAMS developed a module that can create a conceptual suspension model without data from a full multi-body model but with the use of suspension characteristic files where the wheel hub movement e.g. can be entered. A further comparison is shown in table 2.1.

Table 2.1: Technique comparison

Joint	Mass and inertia reduction	Including Suspension Compliance	Multi-Body Reference Model Needed	Vertical Force Analysis of Suspension
Lotus Model	√	√		
Composite Joint	√	√		
Macro Joint	√	√		
Vertical force computation				
3D Installation Ratio				√
Matschinsky				√
Software Packages				
ve-DYNA	√	√	√	
SIMPACK	√	√	√	
ADAMS	√	√		

In general, none of the conceptual suspension modeling techniques gives a clear understanding of the actual suspension kinematics and loads. Forces are applied and processed by the different models, but a full force analysis is missing. Look-up tables are fast and practical in use, but still do not give a force analysis. The derivation of the equivalent vertical force at the contact patch of the wheel does give a force analysis of the suspension. Both the Matschinsky and the installation ratio approach, that is used to obtain the equivalent rates, give relatively good insight in the way forces are acting on the suspension which is also one of the main objectives of this thesis. Forces due to the anti effects during braking and accelerating for example are not included in this force analysis. The logical question now arises which equivalent rate approach is favourable for this thesis project.

The installation ratio method of E. Manes and J. Starkey [9] assumes pure linearised stiffness in order to obtain the wheel rate of the suspension. Actual spring stiffness however is defined as the quotient of the change in spring force and the change in spring elongation. The equivalent spring rate is defined as the quotient of the change in vertical load and the change in vertical displacement of the wheel. The use of linear rates results in an installation ratio derivation that is only applicable for linear springs. Because nonlinear springs are also common in vehicle suspensions an installation ratio must be found that is applicable for both. Another linearisation that E. Manes and J. Starkey make is the relation for the spring elongation f.

$$f = \triangle_E \cos\theta_S \tag{2.27}$$

Referring back to figure 2.12 one can see that this assumption is not valid for larger values of vertical wheel displacement (as is assumed). Finally, no information is given about the preload of the spring and how to implement this force into the installation ratio derivation. More about preload will be discussed in section 3.1.2.

The approach of Wolfgang Matschinsky [2] uses the derivative of the vertical force to the vertical displacement to obtain the equivalent stiffness c_{FA}. This implies that the stiffness c_{FA} is applicable for both linear and nonlinear springs. No linearised limitations, as (2.27), are used which implies that the approach of Matschinsky is also applicable for larger values of vertical wheel displacement. During the conceptual design of a suspension only a certain amount of parameters are available, namely the dimensions of the suspension links, the position and orientation of the spring, etc. In short, the geometry of the suspension. Looking back at the relation for c_{FA} of Matschinsky, the rate is a function of the velocity ratios, v_a/v_{MZ} and v_b/v_{MZ}.

$$c_{FA} = c_F \left(\frac{b}{a}\right)^2 + F_F \left[-\left(\frac{b}{a^2}\right)\left(\frac{v_a}{v_{MZ}}\right) + \left(\frac{1}{a}\right)\left(\frac{v_b}{v_{MZ}}\right)\right] \tag{2.28}$$

Velocity components of a suspension have to be measured and are simply not available in the conceptual design stage because there is no time variable. The velocity ratios however can be obtained by determining the derivatives $\frac{da}{ds}$ and $\frac{db}{ds}$. The latter derivative will not be a trivial one to determine because b is not directly a function of s. There is no information available of how the reduced rates of Matschinsky have to be implemented. Nor is there any information of how to implement dynamic behaviour during braking for example. The same applies for the installation ratio method.

Thus with the objectives in mind, the conceptual model will contain a wheel rate that is obtained using a new equivalent spring stiffness derivation instead of a look-up table based stiffness for example. This is done in order to understand the kinematic behaviour of the suspension. The equivalent stiffness must be applicable for both linear and nonlinear springs. The relation must also be applicable for small and larger vertical wheel displacements. In addition, the relation can not have any velocity dependency and must only contain geometric terms to comply with the conceptual design requirements. Furthermore, a method must be developed to define the position and orientation of the wheel in order to include the correct kinematics and dynamics (during braking).

Chapter 3

Equivalent Stiffness and Damping

Before the conceptual suspension can be realized, equivalent stiffness and equivalent damping must be developed. Starting with the equivalent spring stiffness. As mentioned before, the derivation of the equivalent stiffness can not have any linear assumptions. Thus first a nonlinear approach must be developed in order to be able to implement both linear and nonlinear suspension stiffness. No literature is found that describes the implementation of pre-deflection and pre-load. Thus a relation must also be found for the equivalent pre-deflection as a function of the pre-deflection of the suspension spring.

3.1 Equivalent Stiffness for Linear and Nonlinear Springs

To understand what the equivalent stiffness and damping implies, a graphical overview of a two dimensional trailing arm suspension is shown in figure 3.1.

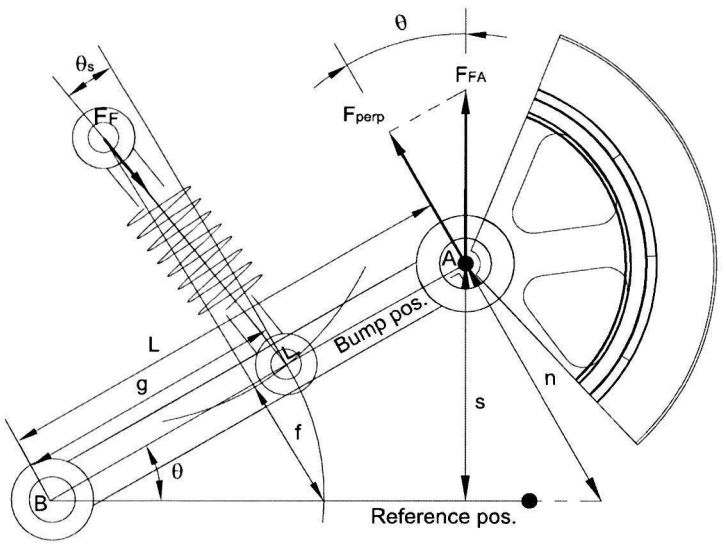

Figure 3.1: Vertical and perpendicular force

The equivalent stiffness c_{FA} of a suspension is basically the vertical stiffness positioned directly above the wheel center A. The stiffness is dependent on the vertical force F_{FA} and the vertical displacement of the wheel s caused by the physical spring and the geometry of the suspension. This equivalent stiffness differs from the stiffness of the physical spring c_F due to its different position and orientation. The stiffness of the physical spring is dependent on the spring force F_F and the spring elongation f. The stiffness of the equivalent spring c_{FA} and the physical spring c_F is defined as:

$$c_{FA} = \frac{dF_{FA}}{ds} \tag{3.1}$$

$$c_F = \frac{dF_F}{df} \tag{3.2}$$

Before relating the physical spring stiffness to the equivalent spring stiffness, a relation must be found for c_{FA} as a function of the perpendicular stiffness c_{perp} at the wheel center. This perpendicular stiffness is dependent on the force F_{perp} positioned perpendicular to the trailing arm and the perpendicular displacement n.

$$c_{perp} = \frac{dF_{perp}}{dn} \tag{3.3}$$

The balance of moments about the pivot center B is obtained in order to relate F_{perp} to F_{FA}.

$$F_{perp}\, L = F_{FA}\, L \cos\theta \tag{3.4}$$

$$F_{FA} = \frac{F_{perp}}{\cos\theta} \tag{3.5}$$

The relation (3.5) can now be used to obtain dF_{FA}/ds. This change in force can be computed using the quotient rule of differentiating. The equivalent spring stiffness can then be written as:

$$c_{FA} = \frac{dF_{FA}}{ds} = \frac{1}{\cos\theta}\frac{dF_{perp}}{ds} + F_{perp}\frac{\sin\theta}{\cos^2\theta}\frac{d\theta}{ds} \tag{3.6}$$

Keeping (3.3) in mind, the first quotient dF_{perp}/ds can be rewritten.

$$\frac{dF_{perp}}{ds}\frac{dn}{dn} = \frac{dF_{perp}}{dn}\frac{dn}{ds} \tag{3.7}$$

The equivalent spring stiffness is eventually a function of the change in s and the change in f or df/ds. The relation $s = L\sin\theta$ includes the variable θ and with the assumption that L is constant, this relation can be used to compute $d\theta/ds$.

$$\frac{d\theta}{ds} = \frac{1}{L\cos\theta} \tag{3.8}$$

Substituting (3.7) and (3.8) into (3.6) gives a new relation for c_{FA} which is now a function of the perpendicular stiffness c_{perp}.

$$c_{FA} = c_{perp} \frac{1}{\cos\theta} \frac{dn}{ds} + F_{perp} \frac{\sin\theta}{\cos^2\theta} \frac{1}{L\cos\theta} \tag{3.9}$$

The main objective is to find a relation for c_{FA} that is a function of c_F. In order to do so, a relation must be found for c_{perp} that is dependent of c_F. The moment equilibrium about pivot point B is used to find a relation for the spring force F_F as a function of the perpendicular force F_{perp}.

$$F_F \, g\cos\theta_s = F_{perp} \, L \tag{3.10}$$

$$F_F = F_{perp} \frac{L}{g\cos\theta_s} \tag{3.11}$$

The stiffness $c_F = dF_F/df$ can now be obtained using (3.11).

$$\frac{dF_F}{df} = \frac{L}{g\cos\theta_s} \frac{dF_{perp}}{df} + F_{perp} \frac{L\sin\theta_s}{g\cos^2\theta_s} \frac{d\theta_s}{df} \tag{3.12}$$

Rewriting dF_{perp}/df gives a new relation for c_F.

$$\frac{dF_{perp}}{df} = \frac{dF_{perp}}{dn} \frac{dn}{df} \tag{3.13}$$

$$c_F = c_{perp} \frac{L}{g\cos\theta_s} \frac{dn}{df} + F_{perp} \frac{L\sin\theta_s}{g\cos^2\theta_s} \frac{d\theta_s}{df} \tag{3.14}$$

Isolating c_{perp} gives:

$$c_{perp} = c_F \frac{g\cos\theta_s}{L} \frac{df}{dn} - F_{perp} \frac{\sin\theta_s}{\cos\theta_s} \frac{d\theta_s}{dn} \tag{3.15}$$

The stiffness c_{perp} is now written as a function of c_F and can be used in relation (3.9) to obtain the equivalent spring stiffness as a function of c_F.

$$c_{FA} = \left\{ c_F \frac{g\cos\theta_s}{L} \frac{df}{dn} - F_{perp} \frac{\sin\theta_s}{\cos\theta_s} \frac{d\theta_s}{dn} \right\} \frac{dn}{ds} \frac{1}{\cos\theta} + F_{perp} \frac{\sin\theta}{\cos^2\theta} \frac{1}{L\cos\theta} \tag{3.16}$$

$$c_{FA} = c_F \frac{g\cos\theta_s}{L\cos\theta} \frac{df}{ds} + F_{perp} \left\{ \frac{\sin\theta}{\cos^2\theta} \frac{1}{L\cos\theta} - \frac{\sin\theta_s}{\cos\theta\cos\theta_s} \frac{d\theta_s}{ds} \right\} \tag{3.17}$$

Using (3.11) to relate F_{perp} with F_F gives:

$$c_{FA} = c_F \frac{g\cos\theta_s}{L\cos\theta}\frac{df}{ds} + F_F\left\{\frac{g\cos\theta_s\sin\theta}{L^2\cos^3\theta} - \frac{g\cos\theta_s\sin\theta_s}{L\cos\theta\cos\theta_s}\frac{d\theta_s}{ds}\right\} \tag{3.18}$$

The relation for the equivalent spring stiffness includes the terms $g\cos\theta_s$ and $L\cos\theta$. Figure 3.2 shows the graphical representation of these terms where:

$$b = g\cos\theta_s \tag{3.19}$$
$$a = L\cos\theta \tag{3.20}$$

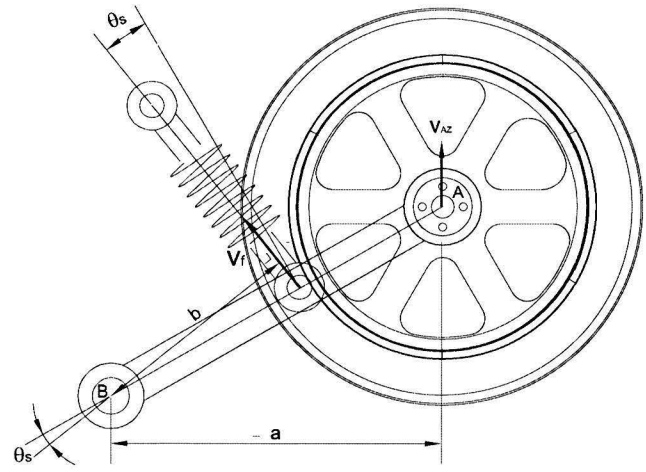

Figure 3.2: Graphical representation of the first fraction

The figure includes the velocity along the axis of the spring v_f and the vertical velocity of the wheel v_{AZ}. Substituting (3.19) and (3.20) in (3.18) results in a new expression for the equivalent spring stiffness.

$$c_{FA} = c_F \frac{b}{a}\frac{df}{ds} + F_F\left\{(\frac{b}{a^2})\,\tan\theta - (\frac{1}{a})\,(g\sin\theta_s\,\frac{d\theta_s}{ds})\right\} \tag{3.21}$$

A 'spring ratio' exists that relates the vertical force at the wheel center with the spring force. The spring ratio can be determined by the moment equilibrium about point B. Reminding (2.7) of the Matschinsky model, the spring ratio can be written as:

$$i_F = \frac{b}{a} = \frac{v_f}{v_{AZ}} = \frac{df/dt}{ds/dt} = \frac{df}{ds} \tag{3.22}$$

Substituting (3.22) into (3.21) results in a new expression for the equivalent spring stiffness.

$$c_{FA} = c_F\, i_F^2 + F_F \left\{ \left(\frac{b}{a^2}\right) \tan\theta - \left(\frac{1}{a}\right) \left(g \sin\theta_s \frac{d\theta_s}{ds}\right) \right\} \tag{3.23}$$

Note that the equivalent stiffness of (3.23) consists of two parts as does the equivalent stiffness of Matschinsky. Both have a first part that is well known and used in the industry and a second part dependent on F_F. Still the derivative $d\theta_s/ds$ is included in the expression. The derivative is difficult to obtain in the conceptual design stage. This derivative has to be written in geometric terms.

3.1.1 The Derivation of $\frac{d\theta_s}{ds}$

There is no direct and simple relation between the the angle θ_s and θ or s. The angle is dependent on the orientation of the spring and the changing length of the spring itself. The derivative $\frac{d\theta_s}{ds}$ is therefore not a trivial one to solve. First a relation for θ_s must be found that is dependent on θ. Figure 3.3 gives the graphical representation of the parameters used to compute the variable θ_s.

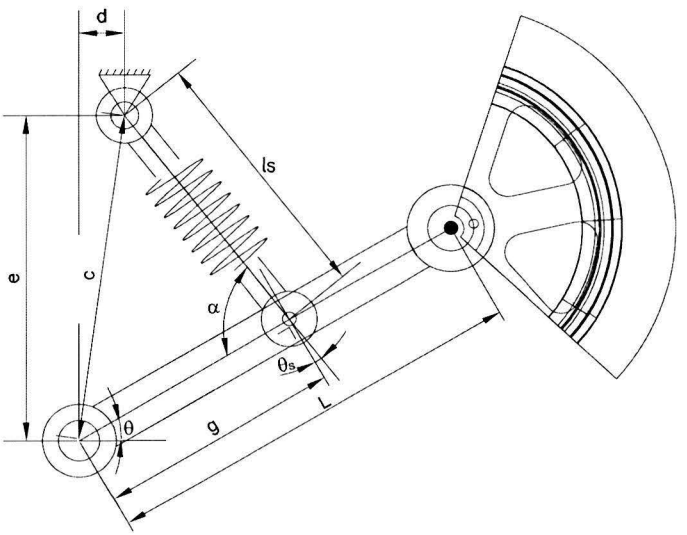

Figure 3.3: Parameters for θ_s calculation

The angle θ of the suspension can be written as a function of the trailing arm length L and the vertical wheel displacement s.

$$\theta = \arcsin\frac{s}{L} \tag{3.24}$$

The spring length l_s is a function of the angle θ as is the spring elongation f.

$$l_s = \sqrt{(g\cos\theta - d)^2 + (e - g\sin\theta)^2} \tag{3.25}$$

$$f = l_0 - l_s \tag{3.26}$$

Where l_0 equals the spring length in starting position $\theta = 0$. Looking closer at figure 3.3 one can see that the parameters g, c and l_s form the sides of a triangle. The distance c can be obtained in two ways which can then be used to obtain the angle α.

$$c^2 = g^2 + l_s^2 - 2gl_s \cos\alpha \tag{3.27}$$
$$c^2 = d^2 + e^2 \tag{3.28}$$

Using this cosine rule a relation can be derived for the angle α.

$$\alpha = \arccos \frac{g^2 + l_s^2 - d^2 - e^2}{2gl_s} \tag{3.29}$$

The angle θ_s can finally be written as:

$$\theta_s = \frac{\pi}{2} - \alpha \tag{3.30}$$

The derivative $\frac{d\theta_s}{ds}$ can be written as:

$$\frac{d\theta_s}{ds} = \frac{d\theta_s}{d\theta}\frac{d\theta}{ds} \tag{3.31}$$

Using (3.29) a relation for $\cos\alpha$ is found which is a function of the angle θ. The derivative $d\alpha/d\theta$ then becomes:

$$\cos\alpha = \frac{g^2 + l_s^2 - d^2 - e^2}{2gl_s} = f(\theta) \tag{3.32}$$
$$\frac{d\cos\alpha}{d\alpha}\, d\alpha = \frac{df(\theta)}{d\theta}\, d\theta \tag{3.33}$$
$$-\sin\alpha\, d\alpha = \frac{df(\theta)}{d\theta}\, d\theta$$
$$\frac{d\alpha}{d\theta} = -\frac{df(\theta)}{d\theta}\frac{1}{\sin\alpha} \tag{3.34}$$

The angle θ_s is determined through the angle α. This relation can also be used to find the solution for the derivative $\frac{d\alpha}{d\theta}$.

$$\frac{d\theta_s}{d\theta} = \frac{d(\pi/2 - \alpha)}{d\theta} = \frac{d(\pi/2)}{d\theta} - \frac{d\alpha}{d\theta} \tag{3.35}$$
$$\frac{d\theta_s}{d\theta} = -\frac{d\alpha}{d\theta} \tag{3.36}$$

There are two relations found for the derivative $d\alpha/d\theta$. These relations (3.34) and (3.36) can now be used to form the relation for the derivative $d\theta_s/d\theta$.

$$\frac{d\theta_s}{d\theta} = \frac{df(\theta)}{d\theta}\frac{1}{\sin\alpha} \tag{3.37}$$

The function $f(\theta)$ equals $\cos\alpha$. When implementing the spring length l_s into the function the following relation emerges.

$$f(\theta) = \frac{-d^2 - e^2 + g^2 + (g\cos\theta - d)^2 + (e - g\sin\theta)^2}{2g\sqrt{(g\cos\theta - d)^2 + (e - g\sin\theta)^2}} \tag{3.38}$$

The derivative $\frac{df(\theta)}{d\theta}$ can now be computed.

$$\frac{df(\theta)}{d\theta} = \frac{y(2g\sqrt{x}) - \frac{gy(-d^2-e^2+g^2+x)}{\sqrt{x}}}{4g^2x} \tag{3.39}$$

$$= \frac{2y\sqrt{x}}{4gx} - \frac{y(-d^2 - e^2 + g^2 + x)}{4gx\sqrt{x}} \tag{3.40}$$

where

$$x = l_s^2 = (g\cos\theta - d)^2 + (e - g\sin\theta)^2 \tag{3.41}$$

$$y = -2g\sin\theta(g\cos\theta - d) + 2g\cos\theta(e - g\sin\theta) \tag{3.42}$$

Because of the long equations that result from the derivative the definitions for x and y are used. Reminding that $\frac{\sqrt{x}}{x}$ equals $\frac{1}{\sqrt{x}}$ and multiplying the first part with the unit factor $\frac{x}{x}$ gives the following relation.

$$\frac{df(\theta)}{d\theta} = \frac{(x + d^2 + e^2 - g^2)y}{4gx\sqrt{x}} \tag{3.43}$$

The derivative of equation (3.37) can now be expressed as:

$$\frac{d\theta_s}{d\theta} = \frac{(x + d^2 + e^2 - g^2)y}{4gx\sqrt{x}}\frac{1}{\sin\alpha} \tag{3.44}$$

Substituting (3.44) and (3.8) in (3.31) gives the expression for $d\theta_s/ds$.

$$\frac{d\theta_s}{ds} = \frac{1}{L\cos\theta\sin\alpha}\frac{(x + d^2 + e^2 - g^2)y}{4gx\sqrt{x}} \tag{3.45}$$

The term $\sin\alpha$ can be written as $\cos\theta_s$. Substituting (3.45) in (3.23) results in the final expression for the equivalent spring rate.

$$c_{FA} = c_F\, i_F^2 + F_F \left\{ \left(\frac{b}{a^2}\right) (\tan\theta) - \left(\frac{1}{a}\right) \left(\frac{g\tan\theta_s}{a}\, \frac{(l_s^2 + d^2 + e^2 - g^2)y}{4gl_s^3}\right\} \tag{3.46}$$

This expression for the equivalent stiffness is referred to as the **Geometric Equivalent Stiffness.**

3.1.2 Equivalent Pre-deflection and Pre-load

Every spring has a certain length when it is unloaded. This is called the natural length l_n. When mounting the spring into the suspension the spring will be compressed. This compression is called the predeflection f_0 and the force of the spring resulting from this deflection is called the preload F_{F0}. However, the amount of pre-deflection and pre-load used for the actual spring is of course not the same as the predeflection of the equivalent spring s_0 and the preload F_{FA0}. A relation has to be found between these two pre-deflections.

The force that the spring induces changes during the bump and rebound movement of the wheel. The preload of the spring does not change during this movement, it remains a constant additional force. The same applies for the predeflection and equivalent predeflection. Both are constant values and thus not a function of the change in spring ratio with respect to the change in vertical wheel displacement. The additional term dependent on the spring force F_F is therefore excluded from the derivation. The equivalent spring stiffness c_{FA} now becomes:

$$c_{FA} = c_F\, i_F^2 \tag{3.47}$$

$$\frac{dF_{FA}}{ds} = \frac{dF_F}{df}\, i_F^2 \tag{3.48}$$

Isolating the equivalent predeflection results in:

$$ds = \frac{F_{FA0}}{F_{F0}}\, \frac{1}{i_F^2}\, df \tag{3.49}$$

Substituting the spring ratio of (3.22) results in the final expression for the equivalent predeflection:

$$s_0 = \int_0^{f_0} \frac{1}{i_F}\, df \tag{3.50}$$

In other words, the equivalent predeflection equals the surface beneath the $\frac{1}{i_F}(f)$ curve from $f = 0$ to $f = f_0$.

3.2 Modified Installation Ratio for Linear Springs

The spring force is a variable within the geometric equivalent stiffness expression that is not based on suspension geometry. This force can easily be implemented by the use of mathematical functions that describe the force/elongation characteristic of the suspension spring. For conceptual design however it is sometimes easier to use a formulation such as the installation ratio. During the design of a suspension the equivalent vertical stiffness, or wheel rate, is determined. The relation between the equivalent spring stiffness and the actual spring stiffness is described within this installation ratio. So if the stiffness of the actual spring must be chosen during the design stage of a suspension, one can easily use the installation ratio i: $c_F = \frac{c_{FA}}{i^2}$. The force/deflection characteristic of the spring can then be obtained from this c_F curve. However, the installation ratio of [9] is only applicable for small angular deflections. In addition, the geometric equivalent stiffness has the spring force F_F as a second unknown variable.

In order to avoid the additional force term no derivative of the force F_{FA} can be used. Therefore, the equivalent spring rate c_{FA}, is now defined as the quotient of the vertical force F_{FA} and the vertical wheel displacement s. The perpendicular rate c_{perp} is defined as the quotient of the perpendicular force F_{perp} and the length n. The rate of the actual spring c_F is defined as the quotient of the spring force F_F and the spring elongation f.

$$c_{FA} = \frac{F_{FA}}{s} \tag{3.51}$$

$$c_{perp} = \frac{F_{perp}}{n} \tag{3.52}$$

$$c_F = \frac{F_F}{f} \tag{3.53}$$

An important aspect that has to be investigated is how to relate the physical spring with the equivalent spring. A solution can be found in the perpendicular length from the lower mounting point of the spring to the horizontal as can be seen in figure 3.4. This perpendicular length $\triangle_e$ can be related to n by:

$$\tan\theta = \frac{n}{L} = \frac{\triangle_e}{g} \tag{3.54}$$

The spring force is zero when the suspension is in the reference position. If a relation can be found for f as a function of $\triangle_e$ then a relation is found between c_F and c_{perp} using equation (3.54). Figure 3.4 shows two triangles, $\triangle Dpt$ and $\triangle Dqr$. Because the triangles have parallel sides, a ratio **R** exists between these sides of the two triangles. The ratio of length $\frac{rq}{tp}$ equals $\frac{Dr}{Dt}$.

$$\mathbf{R} = \frac{rq}{tp} = \frac{\triangle_e \tan\theta_s}{f\sin\theta_s} = \frac{\triangle_e}{f\cos\theta_s} = \frac{Dr}{Dt} \tag{3.55}$$

$$\tag{3.56}$$

From (3.54) the length $\triangle_e$ can be obtained and can be used to create the final expression for **R**.

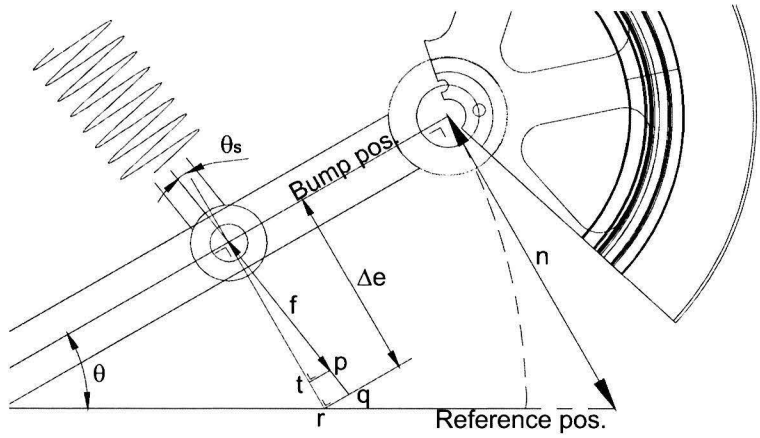

Figure 3.4: The uniform triangles approach

$$\mathbf{R} = \frac{g \tan\theta}{f \cos\theta_s} \tag{3.57}$$

Now the relation for f as a function of $\triangle_e$ is derived. Isolating $\triangle_e$ and substituting it into (3.54) results in the final expression for the spring elongation f.

$$f = n \frac{g}{L \cos\theta_s \, \mathbf{R}} \tag{3.58}$$

Equation (3.58) includes the perpendicular deflection n at the wheel center. The goal for now is to find an equivalent spring rate that includes the force F_{perp}. Substituting (3.11) in the definition of the spring rate $c_F = F_F/f$ and combining it with (3.52) results in a relation between c_F and c_{perp}.

$$c_{perp} = c_F \, (\frac{g}{L})^2 \, \frac{1}{\mathbf{R}} \tag{3.59}$$

Substituting the relation for the vertical displacement, $s = n\cos\theta$, the vertical force (3.5) and the perpendicular rate (3.59) into the equivalent spring rate $c_{FA} = F_{FA}/s$ results in:

$$c_{FA} = c_F \, (\frac{g}{L})^2 \, \frac{1}{\cos^2\theta \, \mathbf{R}} \tag{3.60}$$

If the expression (3.57) for the ratio **R** is substituted in (3.60) the relationship between the spring rate c_F and the equivalent spring rate c_{FA} can be found.

$$c_{FA} = c_F \, i_F^2 \, \frac{f}{g \tan\theta \cos\theta_s} \tag{3.61}$$

The equivalent spring rate is now written as a function of geometric terms without the additional term dependent of F_F. The rate is now also a function of the stiffness c_F of the physical spring. The relation between the equivalent spring rate and the physical spring rate is described by the **Modified Installation Ratio** i_R.

$$i_R = i_F \sqrt{\frac{f}{g \tan\theta \cos\theta_s}} \tag{3.62}$$

This modified installation ratio results in the final expression for the equivalent spring rate:

$$c_{FA} = i_R^2 \, c_F \tag{3.63}$$

Modification Factor

The part of the modified installation ratio after i_F, called the 'Modification Factor (MF)', is a correction factor which includes the actual spring elongation. If a closer look is taken at (3.62) one can imagine the doubt that arises caused by the fraction being a quotient. What happens if the suspension is exposed to very small angular deflections? A result will be that the spring elongation f as well as the angle θ will approach zero, while the angle θ_s will be nonzero. The modified installation ratio, equivalent spring rate, e.g. will also approach zero. The modification factor should approach the value 'one' for small angular deflections. L'Hopital's rule is used to prove that the limit of the modification factor, for θ approaching zero, actually will become 'one'.

$$\lim_{\theta \to 0} \sqrt{\frac{f}{\triangle_e \cos\theta_s}} = 1 \tag{3.64}$$

The derivation of this limit is given in appendix B.1.

3.2.1 Equivalent Predeflection and Preload

The equivalent pre-deflection s_0 and the pre-deflection of the actual spring can be written as:

$$f_0 = \frac{F_{F0}}{c_F} \tag{3.65}$$

$$s_0 = \frac{F_{FA0}}{c_{FA}} \tag{3.66}$$

Substituting (3.63) and (3.65) results in:

$$s_0 = \frac{F_{FA0}}{i_R^2 \, c_F} = \frac{F_{FA0}}{i_R^2 \, \frac{F_{F0}}{f_0}} \tag{3.67}$$

Substituting the spring ratio of (2.7) into (3.67) results in the final expression for the equivalent pre-deflection.

$$s_0 = \frac{i_F}{i_R^2} f_0 \tag{3.68}$$

The relation for the pre-deflection of the equivalent spring is given in equation (3.68). Now that this pre-deflection is known, it can easily be added to the vertical wheel deflection s of the equivalent spring.

3.3 Equivalent Damper Rate for Linear and Nonlinear Dampers

The equivalent damper rate is derived using the linear method of Matschinsky resulting in:

$$k_{DA} = \frac{F_{DA}}{v_{DA}} \tag{3.69}$$

$$k_{DA} = k_D \, i_D^2 \tag{3.70}$$

Because the linear rate of the damper is a function of instantaneous values instead of the change in values, the equivalent damper rate k_{DA} is only applicable for the implementation of linear damper rates. Linear relations as (2.13) can not be used to obtain the damper rate of a nonlinear damper. Similar as for the equivalent spring stiffness derivation, the damper and equivalent damper rate then become:

$$k_D = \frac{dF_D}{dv_D} \tag{3.71}$$

$$k_{DA} = \frac{dF_{DA}}{dv_{DA}} \tag{3.72}$$

Nonlinear damping characteristics ($F_D(v_D)$) often include a different course during bump then during rebound. Implementing such a characteristic into the conceptual suspension model is done by creating different force/velocity functions of the positive and negative velocity range. The linear and nonlinear damper characteristic used in the SimMechanics models are implemented using functions. The nonlinear damping characteristic is given in appendix D.3. The nonlinear damper rate k_D is obtained by differentiating the damper force to the damper velocity. In this thesis however, the equivalent damper rate k_{DA} en the resulting equivalent damper force F_{DA} are obtained by using relation (3.69) and (3.70).

Evaluation of the equivalent stiffness

The expression for the geometric equivalent stiffness is applicable for both linear and nonlinear springs. It is also applicable for larger values of vertical wheel displacement. Relation (3.46) is a function of geometric terms and this makes the geometric equivalent stiffness functional for the conceptual design stage of a vehicle suspension.

Similarities with the equivalent stiffness of Matschinsky are noticed before. The parts that are different from the geometric equivalent stiffness are the velocity ratios. Matschinsky makes use of the equality between the derivatives da/ds and db/ds and the ratios v_a/v_{MZ} and v_b/v_{MZ}. The derivatives are computed in appendix C.2 and C.3 and result in:

$$\frac{da}{ds} = -\tan\theta \tag{3.73}$$

$$\frac{db}{ds} = -\frac{g\sin\theta_s}{L\cos\theta\cos\theta_s}\,\frac{(l_s^2+d^2+e^2-g^2)y}{4gl_s^3} \tag{3.74}$$

Substituting these derivatives in (2.12) of Matschinsky results in exactly the same expression for the equivalent spring stiffness of (3.46). However, in order to perform the derivative calculation, the derivative $d\theta_s/d\theta$ is needed. Matschinsky does not include this derivation in his description of the vertical stiffness. Furthermore, the stiffness perpendicular to the trailing arm c_{perp} is included in the derivation of the geometric equivalent stiffness.

The modified installation ratio is also more than capable of calculating the equivalent stiffness of a two dimensional trailing arm. In comparison to the method of Matschinsky and the geometric equivalent stiffness, the method using the modified installation ratio is practically more appealing. The mathematical aspect of the derivation is simple and by using geometrical terms, the method is also applicable for conceptual design. The modified installation ratio is also applicable for large angular deflections of the trailing arm. However, to avoid the additional force term of Matschinsky and the geometric equivalent stiffness, linearized rate definitions are assumed. Therefore, the modified installation ratio is only applicable for linear spring stiffness where Matschinsky and the geometric equivalent stiffness are applicable for both linear and nonlinear spring stiffness.

Chapter 4

Multi-body Reference and Conceptual Suspension Model

To validate the theory developed in the previous chapter a reference model of a trailing arm suspension is developed that can be used to check the results. The process of developing this suspension model is described in Appendix D. To realise the validation two multi-body suspension models are created. One model representing the reference suspension and the other representing the conceptual suspension. Both models are created with the MATLAB multi-body toolbox SimMechanics. By creating both multi-body models in the same environment the models can be compared directly instead of having to deal with the differences in modeling programs. The graphical representation of the vehicle model is shown in figure 4.1.

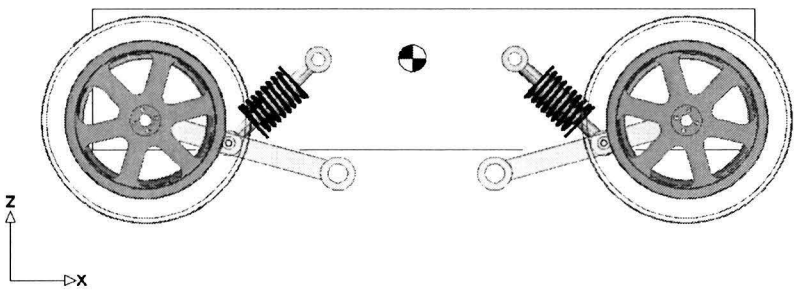

Figure 4.1: Graphical representation of the vehicle model

4.1 Multi-body Reference Model

The general layout of the SimMechanics vehicle model (including the reference suspension model) is given in figure 4.2.

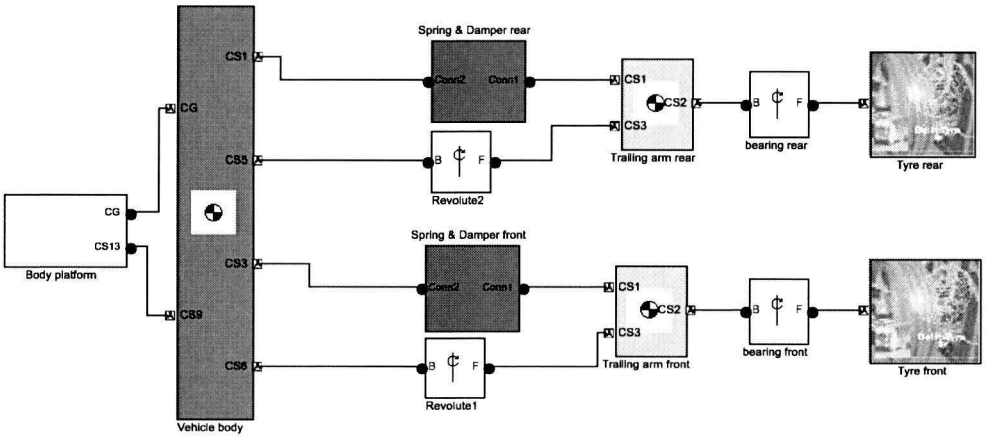

Figure 4.2: General layout suspension model

The model consists of a body platform, vehicle body, trailing arm, wheel and spring/damper combination. The body platform includes the orientation and the degrees of freedom of the vehicle body. It also includes the sensors for measuring the position and velocity of the center of gravity as well as the pitch angle of the vehicle body. The vehicle body includes its mass and inertia as well as the coordinates of the hinges and the connection between the body and the spring/damper combination.

The trailing arm is modeled as a rigid body because the suspension model does not include any compliant parts. The mass and inertia are also neglected which leaves the position and orientation of the arm. The arm is connected to the vehicle body by a revolute joint.

The spring and damper are modeled using a SimMechanics block that basically consists of two point masses connected by a joint that allows the masses to rotate and translate with respect to each other. Function blocks are inserted in this SimMechanics block in order to model linear and nonlinear springs and dampers. Furthermore, a revolute joint acts as a wheel bearing connecting the wheel and trailing arm. The Delft-Tyre model is used to represent the rim and tyre. The rim and tyre contain the properties of the ones used by the URE team.

4.2 Conceptual Suspension Model

4.2.1 Modeling Approach

In order to create the conceptual suspension model the physical trailing arm is replaced by a joint connection. This conceptual joint contains the equivalent stiffness (or wheel rate) and equivalent damping of the suspension acting vertically on the wheel center. Furthermore, the joint connection contains the trajectory of the wheel. The effect that braking has on the suspension is also included within this joint. More about the brake effects and the implementation in the conceptual suspension model is discussed in chapter 4.3. The schematic process from the suspension model to the realization of the conceptual suspension model is shown in figure 4.3.

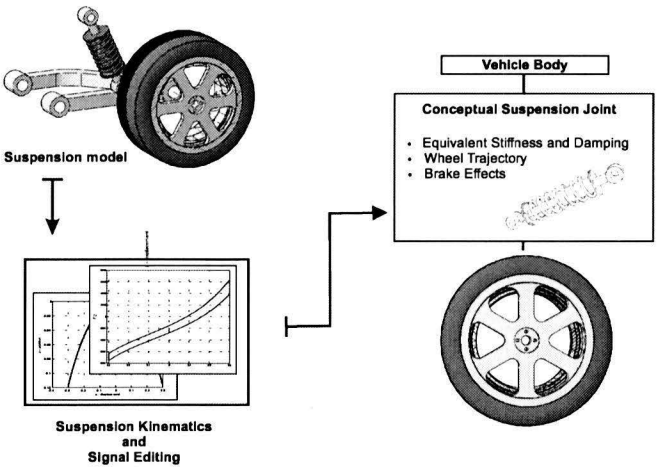

Figure 4.3: Schematic process to the conceptual suspension model

Both suspension models are created in such a way that any configuration of the trailing arm can be entered. The suspension kinematics can be obtained by a kinematic test where the suspension model is subjected to an amount of vertical wheel displacement. More about the kinematic test is discussed in chapter 5. Resulting from this test are the trajectory of the wheel and the force-displacement characteristic. A look-up table is used to implement the trajectory of the wheel. The x data vector of the lookup table must be monotonically increasing so the output signals for this $x(z)$ characteristic must be 'smoothed'. Polynomial fits are used to have a unique mapping of the $x - z$ data.

Other output signals of the kinematic test create the force-displacement or $F(z)$ characteristic which acts vertically on the wheel center. This force signal will not be fitted. The equivalent spring stiffness and damper rate will be used to obtain this vertical force. In addition the smoothing and fitting of the signals, as well as the computation of the variables that are needed to obtain the equivalent stiffness and rate, will be done in a separate m-file. The input signals are now ready to be implemented in the conceptual suspension joint within the SimMechanics model. The conceptual suspension model does not include the physical trailing arm suspension anymore. Instead, the conceptual suspension joint includes the suspension kinematics and brake effects.

4.2.2 SimMechanics Model

The general layout of the SimMechanics vehicle model (including the conceptual suspension joint) is shown in figure 4.4. The model consists of the body platform, a vehicle body, two joint connections and two 'Delft-Tyre' models. The body platform is identical to the one that is used in the suspension model. The vehicle body also has identical mass and inertia properties but also includes the connection points of the joint connection. The wheel must move along the same trajectory as in the suspension model. However, the equivalent spring and damper are always positioned vertically on the wheel center which means that they must move with the trajectory of the wheel. Therefore, the connection of the equivalent spring and damper with the vehicle body cannot be fixed.

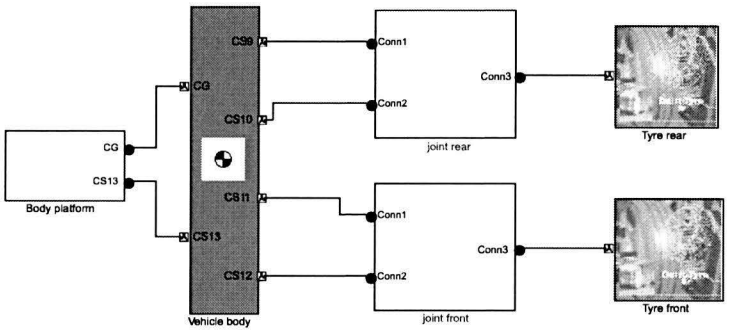

Figure 4.4: General layout conceptual model

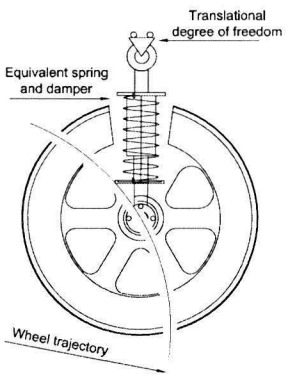

Figure 4.5: Conceptual model

A graphical representation of the conceptual model is given in figure 4.5. The trajectory of the wheel with respect to the vehicle body must be defined and the translational degree of freedom must be included in the joint connection. These elements within SimMechanics are shown in figure 4.6.

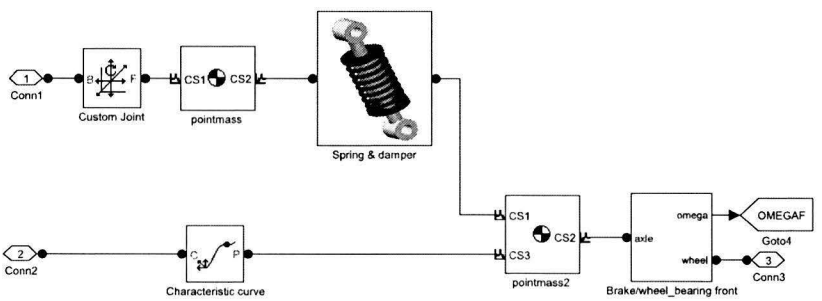

Figure 4.6: Joint connection

The trajectory of the wheel is defined by a point-curve constraint ('characteristic curve'). This joint removes two translational degrees of freedom and allows a body to move along a predefined curve. This curve is the fitted $x(z)$ characteristic that is obtained in the kinematic test. The translational degree of freedom is defined by the custom joint. This joint eliminates all translational and rotational degrees of freedom except for the longitudinal translation. The joint is placed between the vehicle body and the spring/damper combination. Again the spring and damper is defined by two point masses with a joint in between. The masses can only translate in vertical direction with respect to each other. Removing the rotational degree of freedom about the vertical axis will prevent the masses from rotating about each other. Removing the translational degree of freedom in longitudinal direction prevents the masses from moving in x-direction with respect to each other as well as rotating about the y-axis. Two translational and rotational degrees of freedom then remain. The stiffness and damping are defined by look-up tables as can be seen in figure 4.7.

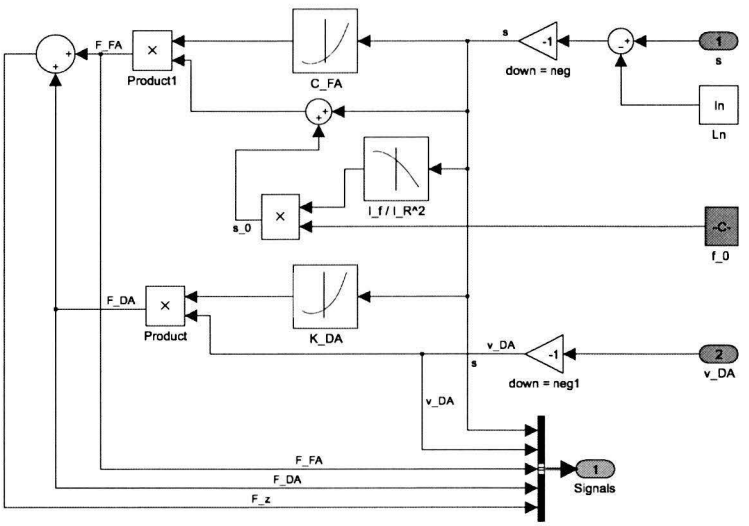

Figure 4.7: Spring and damper force in SimMechanics using the Modified Installation Ratio

This figure shows the implementation of the modified installation ratio and thus the linear spring and damper. The vertical displacement s and the vertical velocity of the wheel v_{DA} are used to obtain the spring and damper force. The equivalent spring force is related with the displacement by $F_{FA} = c_{FA}\, s$ where the total displacement equals the sum of the displacement s and the pre-deflection of the spring s_0. The damper force is related to the velocity by $F_{DA} = k_{DA}\, v_{DA}$. Modeling the equivalent spring and damper force for nonlinear stiffness and damping is also done with lookup tables as can be seen in figure 4.8.

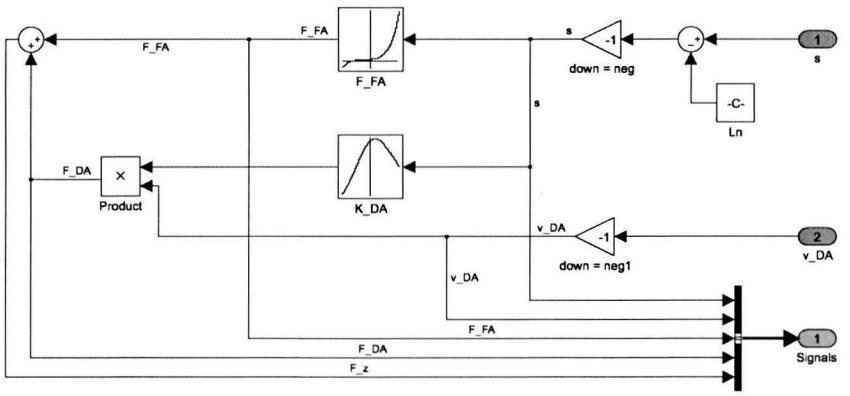

Figure 4.8: Spring and damper force in SimMechanics using the Geometric Equivalent Stiffness

The way in which the damper force is modeled is the same as in figure 4.7. For the equivalent spring however, instead of determining the force from the stiffness table, only one lookup table is modeled that includes the equivalent spring force F_{FA} and pre-load s_0. The vertical force is obtained by integrating the equivalent spring stiffness c_{FA} to the vertical wheel displacement s.

$$F_{FA} = \int_0^{s+s_0} c_{FA}\, ds \tag{4.1}$$

4.3 Braking

The conceptual suspension joint connects the wheel with the vehicle body. The joint also includes the equivalent force induced by the spring and damper caused by submitting a vertical displacement of the wheel. However, what will happen if the joint is implemented in a vehicle body and is submitted to a brake torque? In order to implement braking in the joint the effects on the suspension during braking must be investigated.

4.3.1 Suspension Behaviour during Braking

The load transfer of the vehicle that occurs during braking is discussed and the dimensions of the suspension, with the chosen amount of anti-dive and anti-rise, follow from these design forces and parameters. The challenge lies now in the way of modeling the brake torque and forces within the conceptual suspension model. To model such an effect, a force analysis must be done upon the suspension in order to understand what consequences the brake torque brings. Modern vehicles apply outboard brakes which means that the brake torque is applied within the wheel. These outboard brakes are recognizable by the brake disc or drum inside the wheel. Figure 4.9 shows the forces acting upon the wheel during braking assuming that the brake torque is applied with outboard brakes.

Decelerating a turning wheel is accomplished by applying a torque T_b in opposite direction of the angular velocity ω of the wheel. The load transfer resulting from the deceleration results in an additional vertical force $\triangle F_z$ on the wheel. The brake torque finds its way to the circumference of the wheel where the contact patch of the tyre and the road surface induce a longitudinal brake force F_b together

due to friction between the two materials. The brake torque is guided from the brake caliper to the brake disc. The disc is attached to the wheel and the brake caliper is attached to the trailing arm. The latter causes a reaction torque in opposite direction of the brake torque as can be seen in figure 4.10.

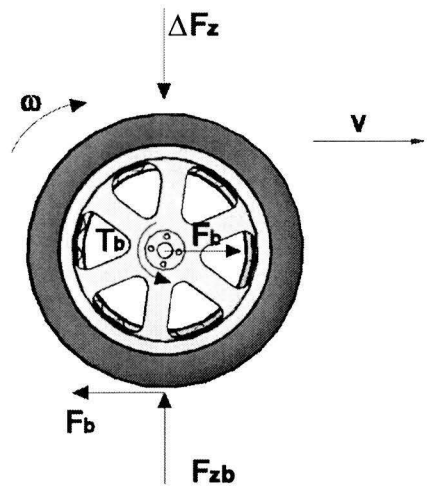

Figure 4.9: Forces upon the front wheel during braking

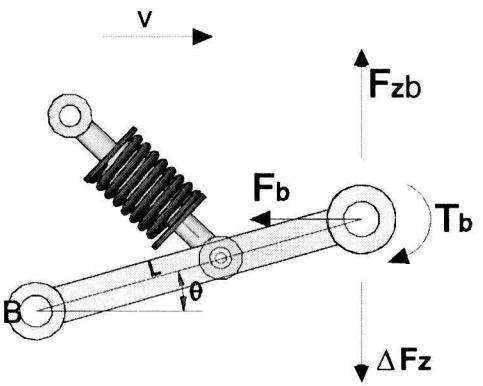

Figure 4.10: Forces upon the front wheel connection during braking

The connection between the wheel and the trailing arm causes a reaction force in opposite direction of the brake force. The load transfer is not computed because the position, orientation and mass properties of the vehicle body are already defined within SimMechanics. However, the reaction force of the transfer load is induced by the spring and damper in the multi-body model. This means that $\triangle F_z$ corresponds to the sum of forces induced by the equivalent spring and damper $(F_{FA} + F_{DA})$. The brake force and torque can be modeled as an additional vertical force. The moment equilibrium about hinge B gives an expression for the new vertical force due to braking F_{zb}.

$$-T_b + F_b\, L \sin\theta - \triangle F_z\, L \cos\theta + F_{zb}\, L \cos\theta \tag{4.2}$$

$$F_{zb} = \frac{T_b}{L \cos\theta} - F_b \tan\theta + (F_{FA} + F_{DA}) \tag{4.3}$$

The expression includes $(F_{FA} + F_{DA})$ and the addition of a vertical force due to braking. This addition means that the slope of the vertical force characteristic does not change, the characteristic will only shift vertically because of the force addition. The term $F_b \tan\theta$ is also not computed in the model. The point-curve block in the SimMechanics model already constraints the path of the wheel like the physical trailing arm does in the reference model. This constraint results in the realisation of the longitudinal reaction force due to F_b.

The same methodology applies for the rear suspension. The direction of forces and torques remain the same, but the direction of moments changes. The force F_{zb}, including the effects due to braking, can be used to model the anti-dive and anti-rise effect and thus the resistance to pitch.

4.3.2 Model implementation

Both suspension models use the same brake system to apply the brake torque. A brake characteristic is used as an input to trigger the brake system. Using the brake distribution p, the correct amount of brake torque will be applied to the front and rear brakes.

The conceptual suspension model has no physical trailing arm and thus no physical attachment for the brake caliper to transfer the brake torque to. The connecting joint of the conceptual suspension model includes a point-curve constraint where the point can rotate rotate freely while following the curve. Therefore, the constraint cannot transfer any torque. A solution to this problem can be found in the spring/damper block of the conceptual model. This block uses two point masses that can translate and rotate with respect to each other as is discussed in paragraph 4.1. The spring/damper block is always positioned vertically above the wheel center and follows its trajectory. In addition, the point masses only translate vertically with respect to each other. Therefore, transferring the brake torque is accomplished by eliminating the rotational degree of freedom about the y - axis between these two point masses.

The additional vertical force due to braking is modeled in the spring/damper block within the joint connection. The additional force due to braking is then added to the vertical force induced by the equivalent spring and damper. Figure 4.11 shows this model.

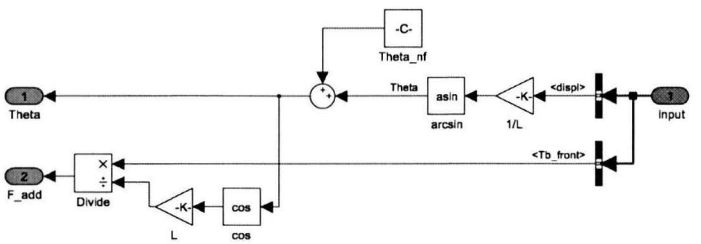

Figure 4.11: Model of the additional vertical force due to braking

Chapter 5

Kinematic and Dynamic Test Results

5.1 Kinematic Test Results

To examine and validate the conceptual model numerical tests must be performed. As mentioned in the introduction the conceptual suspension model will be subjected to a kinematic test and a dynamic test. The dynamic test will be discussed in chapter 5.2. Both the reference model and the conceptual model will be subjected to the exact same excitations in order to compare the results. For the kinematic test the models are fixed in space and the trailing arm is positioned horizontally, i.e. $\theta = 0\ rad$. The natural length of the spring is the calculated length at $\theta = 0\ rad$ and a certain pre-deflection is added to this length. Both the linear and nonlinear stiffness and rates are implemented using functions. The attached wheel is subjected to an unconventional large amount of vertical displacement of $0.3\ m$, both bump and rebound, to see if the conceptual suspension model is accurate for a large angular deflection. The first step is to compare the kinematics of both models and thus excluding any spring or damper force at first. The trajectories $x(z)$ of both models are measured and compared.

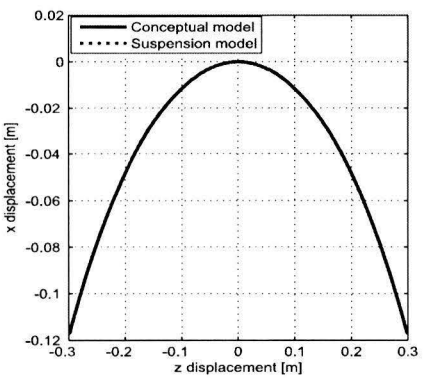

Figure 5.1: Results of the wheel trajectory

The comparison is shown in figure 5.1. The results for the wheel trajectory of the two models overlap each other which means that the process of signal editing and the definition of the wheel trajectory with the point-curve constraint work properly. The next step is to compare the different equivalent force methods. The spring and damper of the reference suspension model are activated and the kinematic test upon this model is done again. The resulting variables as vertical displacement

of the wheel center, spring force, piston velocity, etc are used as an input in MATLAB to compute the different equivalent spring and damper forces. The comparison is performed including the following methods:

- *Modified Installation Ratio*
- *Geometric Equivalent Stiffness*
- *Matschinsky*
- *Standard Installation Ratio*

The approach of E. Manes and J. Starkey [9] is applied to the trailing arm suspension. This results in an installation ratio i_{FS}. Because the industry also uses this ratio, it is referred to as the **Standard Installation Ratio**. The implementations of the different equivalent force methods in MATLAB are discussed in appendix A. The kinematic tests include the implementation of a linear and nonlinear spring as well as a linear and nonlinear damper.

5.1.1 Linear Suspension Spring and Damper

The first kinematic test involves the implementation of a linear spring and damper. The resulting $F(z)$ characteristic of the reference suspension model is then compared with the characteristics of the conceptual suspension model. The method used to obtain the equivalent damper rate is the same for all four cases.

Damping and preload excluded

The damping is excluded at first as well as the preload to objectively review the results of the vertical force.

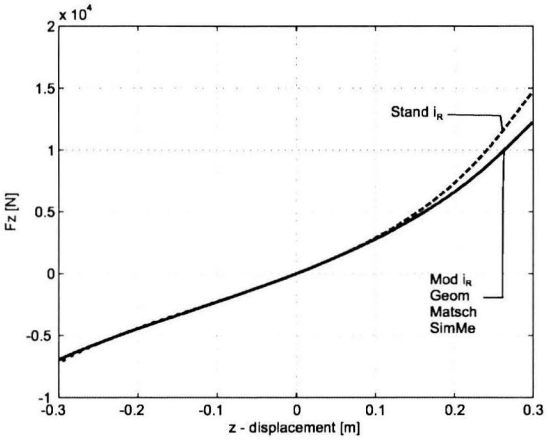

Figure 5.2: F(z) characteristic including a linear spring

Figure 5.2 shows the result of the kinematic test. It is clearly seen that the $F(z)$ curves of the modified installation ratio, geometric equivalent stiffness and Matschinsky follow the $F(z)$ curve of the suspension model very accurately. The difference in vertical force (or error) between the reference model and the four different methods is also computed.

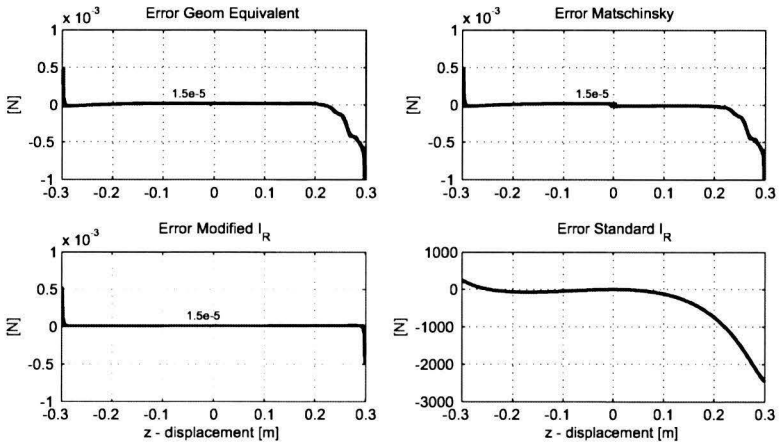

Figure 5.3: Error with respect to the reference model

Figure 5.3 shows the difference in vertical force with respect to the reference model. The method of the standard installation ratio results in the largest difference in vertical force. The expressions for the equivalent stiffness of the other methods follow the change in geometry of the suspension, during bounce and rebound, very good. Needless to say, these results are extremely accurate. The result for the standard installation ratio however, is far from accurate. The difference in vertical force varies and the maximum difference is 2436 N. The error also grows with increasing vertical deflection. This is caused by the linearised assumption that E. Manes and J. Starkey make for the spring elongation. However, in the range of -0.1 m to 0.1 m, the error seems constant and close to zero. The maximum error within this range is still 115 N.

Damping and preload included

Now the linear damper rate and the pre-deflection are implemented in order to check the total vertical force. The results are shown in figure 5.4.

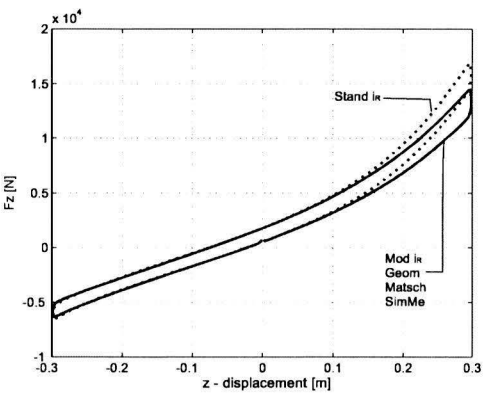

Figure 5.4: F(z) characteristic

The $F(z)$ curves of the modified installation ratio, geometric equivalent stiffness and Matschinsky still follow the $F(z)$ curve of the suspension model very accurately.

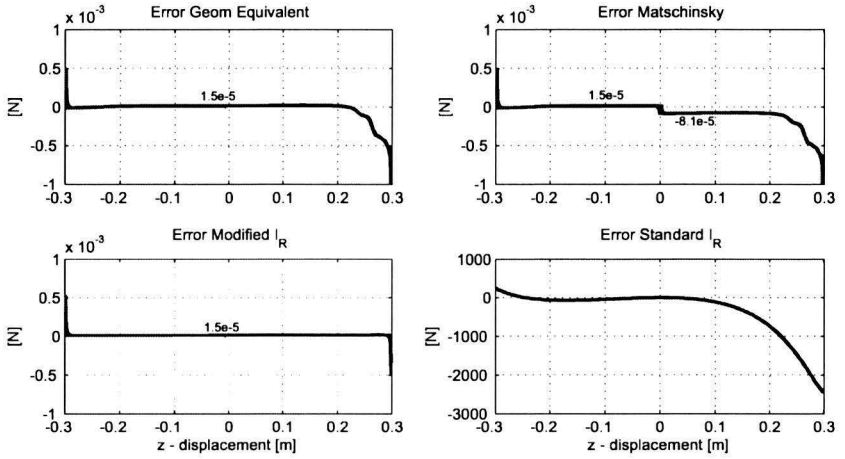

Figure 5.5: Error with respect to the reference model

Figure 5.5 shows the difference in vertical force. The maximum difference remains the same for all methods. This is due to the equivalent damper force that is obtained in the same way for all methods. The figure also shows that these results are also extremely accurate.

Evaluation of the test results

The test results show that the standard installation ratio method is the most inaccurate one. To give an idea of the difference in accuracy a comparison is given in figure 5.6.

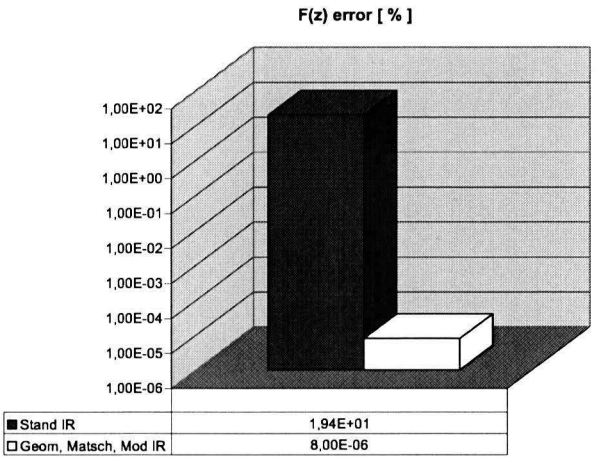

Figure 5.6: Maximum error comparison

This figure shows the maximum error of the vertical force including the damper force and pre-load. The error is displayed in logarithmic scale. The linear assumption for the spring elongation, that the

standard installation ratio makes, results in an inaccurate course of the vertical force as expected before. However one can imagine that a certain percentage of error is acceptable in the process of developing a suspension. In addition, in the case of the standard installation ratio the error becomes smaller for a smaller range of vertical displacement. Hence, this ratio could be accurate enough for vehicles with a small range of vertical displacement such as race cars. The methods of the modified installation ratio, geometric equivalent stiffness and Matschinsky are accurate for vehicles varying from extreme race cars (formula one) to rally or off-the- road cars/trucks. These rally or off-the-road cars/trucks acquire large vertical displacements of the wheel in order to sustain the traction as long as possible (longer wheel/road contact).

5.1.2 Nonlinear Suspension Spring and Damper

The second kinematic test involves the implementation of a nonlinear spring and nonlinear damper rate. The characteristics of the nonlinear springs and dampers are displayed in appendix D.3. Again the damping and pre-load are excluded at first.

Damping and pre-load excluded

The results of the second kinematic test are shown figure 5.7.

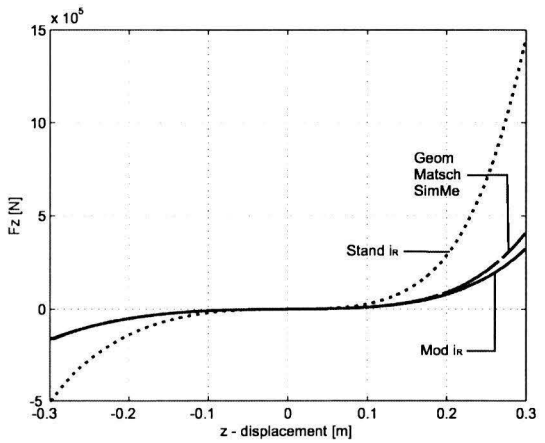

Figure 5.7: F(z) characteristic including a nonlinear spring

In comparison with the results for the implementation of a linear spring, one can see that the result for the modified installation ratio method is inaccurate for larger values of vertical wheel displacement. The same can be determined for the standard installation ratio, the error is out of proportion. The difference in vertical force that is shown in figure 5.8 gives more insight.

The result of the modified installation ratio shows that this method is not accurate for the implementation of a nonlinear spring. In the range of -0.1 [m] to 0.1 m, the error seems constant and close to zero [N]. The maximum error however is still 563 N. The results for the geometric equivalent stiffness method and the Matschinsky method are still very accurate.

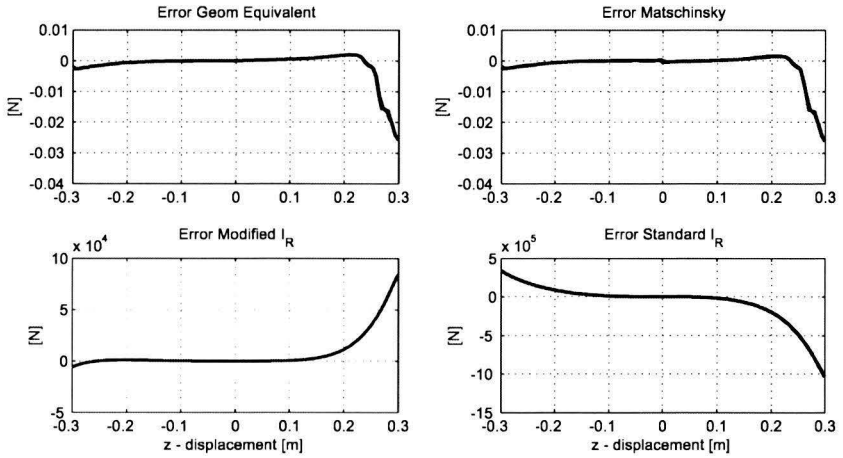

Figure 5.8: Error with respect to the reference model

The results for the standard and modified installation ratios show that the methods are not applicable for the implementation of a nonlinear spring. These methods are therefore excluded from any further analysis. The equivalent pre-load and equivalent damper force are obtained by using the same relations for the remaining two methods. Thus only the geometric equivalent stiffness is analyzed further.

Damping and pre-load included

The equivalent damper force is obtained by linear relations so only the equivalent pre-deflection is included at this point. The difference in vertical force is shown in figure 5.9.

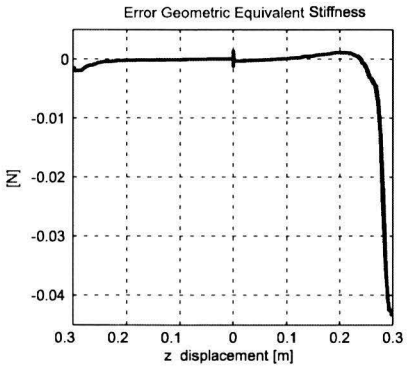

Figure 5.9: Error for a nonlinear spring including pre-load

The $F(z)$ curve of the geometric equivalent stiffness still follows the $F(z)$ curve of the suspension model very good. The error remains about the same as without the equivalent pre-load. Thus relation (3.50) for the equivalent pre-deflection is found to give accurate results. Now damping is included in the comparison. A maximum piston velocity of 1 m/s is submitted in order to reach the nonlinear part of the damper/velocity characteristic. The results are shown in figure 5.10.

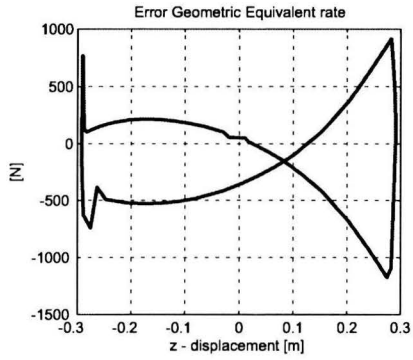

Figure 5.10: Error for a nonlinear spring including pre-load and damping

The hysteresis is caused by the damper resulting in an additional force to the one that is induced by the spring. It is obvious that the relation for the equivalent damper rate is not accurate if a nonlinear damper is implemented. The relation can not follow the nonlinear behaviour of the suspension damper characteristic at larger vertical displacement of the wheel. This explains the twisted curve of the error.

However, reminding the range of vertical force in this situation, the error of 0.26 % is relatively small. The error will increase at higher piston velocities. Therefore, a test is performed where the velocity is raised to reach a maximum of 4 m/s which results in a maximum error of 1 %.

Evaluation of the test results

The test results show that the geometric equivalent stiffness relation and the method of Matschinsky are very accurate. The standard installation ratio is not applicable for nonlinear springs and the modified installation ratio could be used within the vertical displacement range of -0.1 to 0.1 m if a maximum error of 5 % is tolerated. The difference in accuracy of the geometric equivalent stiffness, the Matschinsky method and the modified installation ratio are given in figure 5.11.

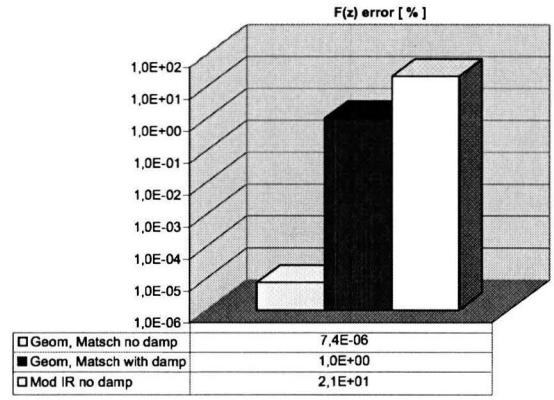

Figure 5.11: Maximum error comparison

The methods of the modified installation ratio and the geometric equivalent stiffness are imple-

mented in two different conceptual suspension models as is described in paragraph 4.2.2. To see if the models are real-time compatible, the CPU time of the reference suspension model has to be compared with the CPU time of the modified installation ratio method and the geometric equivalent rate. Two tests are performed:

- CPU test including a linear spring and a linear damper.
- CPU test including a nonlinear spring and a nonlinear damper.

It is established earlier that the modified installation method is not applicable for nonlinear springs and is thus excluded from the second test. The results of the CPU times are shown in figure 5.12.

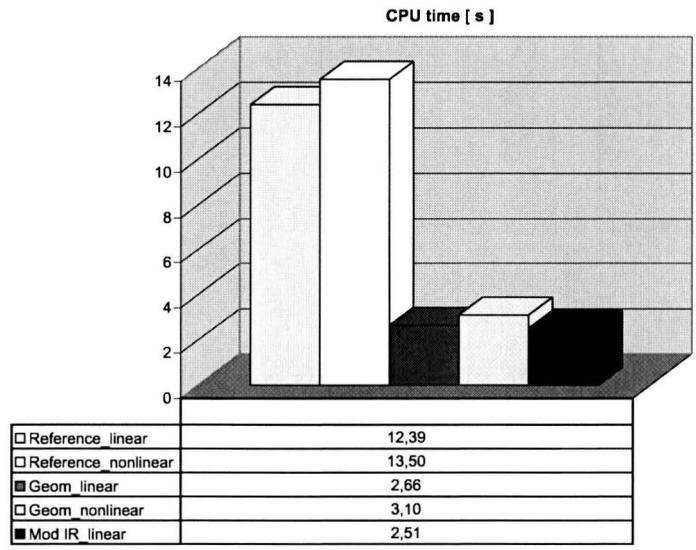

Figure 5.12: CPU time comparison between reference and conceptual model

The simulation is performed over a time span of 9 s. The results clearly show that the CPU time of the reference suspension model exceeds the imposed simulation time. In addition, the CPU time is dependent on the performance of the used computer. The difference in CPU time between the reference and conceptual model is therefore more interesting.

For linear stiffness and damping, the conceptual suspension model including the geometric equivalent stiffness is up to **4.7 times faster** than the reference suspension model. For nonlinear stiffness and damping the conceptual suspension model is **4.4 times faster**. The method of the modified installation ratio also improves the CPU time substantially. The conceptual model including this ratio is even **5 times faster** than the reference model.

One must keep in mind that these CPU times result from a simple kinematic test. The real challenge lies in the dynamic test where more variables have to be taken into account such as the effect due to braking.

5.2 Dynamic Test Results

The kinematics of the conceptual suspension model are tested while the vehicle is fixed in space. The dynamics of the vehicle are even more important and interesting to investigate. The derivation of the equivalent spring stiffness is based on the assumption that the trailing arm is positioned horizontally. The actual suspension model however is designed to be mounted under an angle due to anti-dive and anti-rise. The vertical force F_{FA} is then no longer dependent on the angular deflection θ alone, but also dependent on the initial angle θ_{nf}. The implementation of this aspect into the conceptual suspension model is discussed in appendix B.2. The design of the total suspension model can be found in appendix D. The dynamic test is performed only with the conceptual suspension model including the modified installation ratio. In addition, braking has to be implemented in the conceptual model. Therefore, only one equivalent stiffness method is chosen at first. During the dynamic test two vehicle models, one including the reference suspension model and one including the conceptual suspension model, are subjected to a constant forward velocity of 50 km/h. After two seconds a brake torque is applied to the wheel bearings.

Static test

Preceding to the dynamic brake test a trivial static test is performed. Before running the simulation the suspension is orientated as is designed. During the simulation the weight of the vehicle is working on the equivalent springs and dampers due to gravity. Mistakes in the model can result in a wrong pitch angle, weight distribution, height of the center of gravity, etc. The results for the static test are shown in figure 5.13.

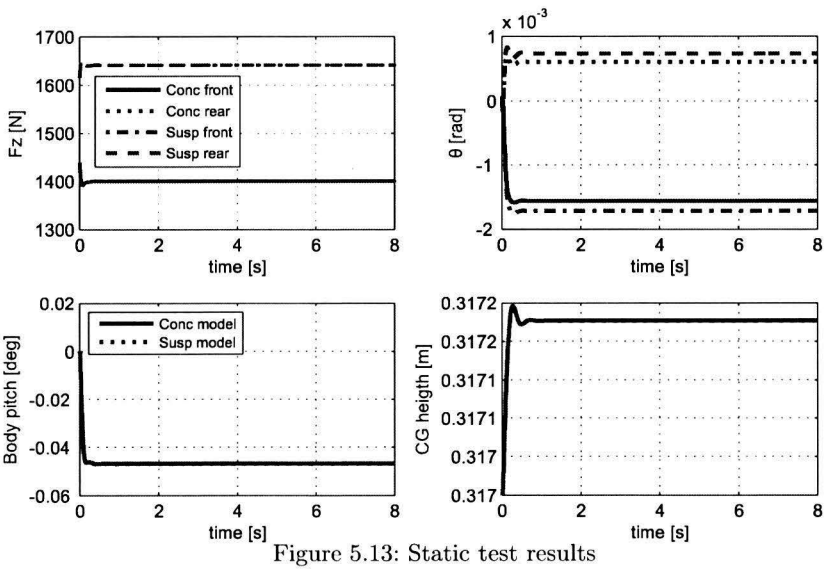

Figure 5.13: Static test results

The values for the angular deflection θ of the suspension for the front and rear are close to zero. This implies that the front and rear suspension of both models have correct and similar initial orientation. The pitch angle of both models and the height of the center of gravity also correspond to the each other. The values for the vertical force F_z are as good as equal to the nominal design force F_N (see table D.4). In addition, the vertical forces of the suspension and the conceptual suspension overlap each other. Looking at the results of the kinematic tests, the accuracy of the static test results are to be expected.

Dynamic test

Now that the model is checked the brake test can be performed. Figure 5.14 shows the results for the velocity of the vehicle and the angular velocity of the wheels. The deceleration of the wheels of both models coincides with each other. This is due to the use of the exact same brake system. No wheel lock occurs and the deceleration of the angular velocity of the wheels causes both vehicle bodies to decelerate as well. This can be seen in the plot of the vehicle velocity.

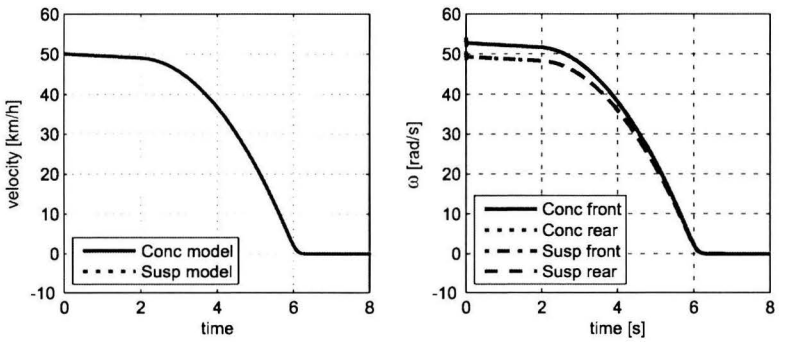

Figure 5.14: Vehicle velocity and angular velocity of the wheels

Another important aspect is the vertical force. The kinematic tests already prove that the modified installation ratio method provides accurate equivalent vertical force results for linear springs and dampers. Thus it is expected that the vertical force results of the dynamic test of both models will coincide.

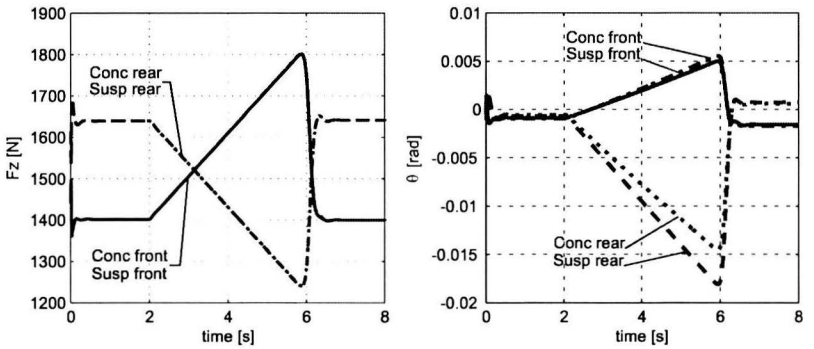

Figure 5.15: Vertical force and angular deflection of the wheels

The left plot of figure 5.15 indeed shows identical courses of F_z for the reference and conceptual suspension model. Braking of the vehicle causes an increases in vertical force at the front and a decrease in force at the rear and thus causing the suspension to deflect. The angular deflection of the conceptual model can not be measured because of the prismatic movement of the wheel with respect to the body. In addition, there is no physical trailing arm to measure this deflection from. In the conceptual model, the angular deflection is obtained by using the true vertical displacement signal s' of the wheel and implementing it in relation (3.24). This can also be seen in figure 4.11. The right plot of figure 5.15 shows the angular deflection θ of the suspension. It shows that both front suspension

deflect almost equally. However, the angular deflection of the rear suspensions shows different plots. The rear wheel of the conceptual suspension deflects less. This translates in less rise of the back of the vehicle. This can be seen in the plot of figure 5.16.

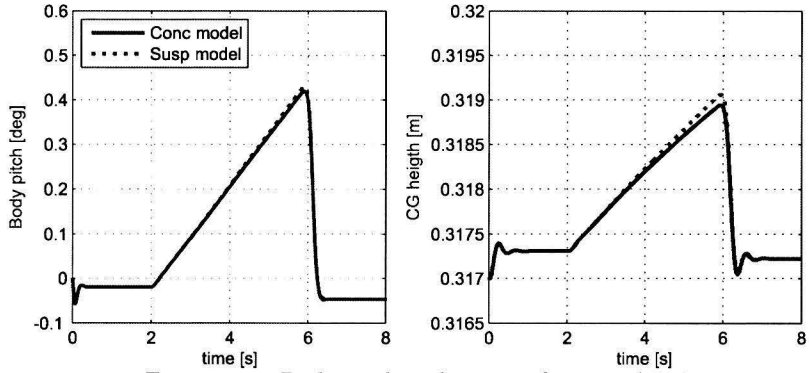

Figure 5.16: Body pitch and center of gravity height

Less rise of the vehicle results in a lower body pitch and a lower maximum height of the center of gravity as is shown in the right plot of figure 5.16. The additional vertical force, that basically increases the vertical force/displacement characteristic of the suspension, has a positive result on the translation of the anti-dive and anti-rise to the conceptual suspension model. Thus it also has a positive effect on the dynamic behaviour of the vehicle model during a brake simulation. Looking back at the derivation of the new vertical force characteristic $F_{zb}(s)$, the dynamics in the suspension due to braking should be implemented as a vertical force characteristic. However, despite the fact that the values for the angular deflection are very small, the relative maximum error between the rear suspensions is 20 %. A solution can be found in appendix B.2 where the initial position of the trailing arm is discussed. In the model, the true vertical displacement s' is implemented in relation (3.24) in order to obtain the angular deflection θ. However, this relation is applicable for s and not s'. More investigation should be done to improve this translation of dynamic brake behaviour to the conceptual suspension model.

Besides the translation of the brake dynamics into the joint connection, the performance of the total conceptual model with respect to the CPU time is investigated.

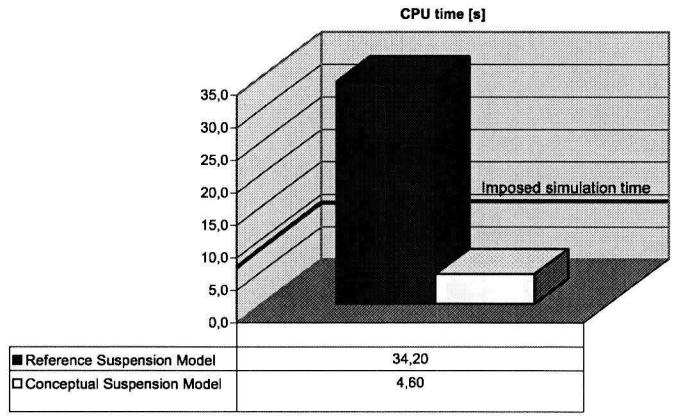

Figure 5.17: CPU time comparison

The imposed simulation time of both models is 8 [s]. An overview of the results is given in figure 5.17. To perform the simulation the reference suspension model requires an average CPU time of $34,2$ s. The conceptual suspension model on the other hand requires an average CPU time of $4,6$ s. The conceptual suspension model is $7,4$ times faster and accounts for an improvement of $86,5$ % with respect to the reference model. In addition, the conceptual model consumes only $57,5$ % of the imposed simulation time. As said before, this depends on the performance of the used computer.

To make sure that the simulation after vehicle stand still does not influence the results of the model performance with respect to the simulation time, a second simulation is done with an imposed time of 5 s. The results show an improvement of 81 % with respect to the reference suspension model. The conceptual suspension model is thus still a great deal faster. The overall improvement of CPU time is $81 - 86\%$. Hence, it is proved that the conceptual model is applicable for real-time simulation.

Chapter 6

Conclusions and Recommendations

In this master thesis the objective was to understand the kinematic behaviour of a vehicle suspension. Furthermore, the objective was to create a suspension model which is applicable in a real-time environment. Having considered the objectives and the literature study, this thesis is focussed on the description of the vertical or equivalent stiffness of the suspension. The description concentrates on the correct characterization of the spring/damper installation ratio. This aspect makes it possible to relate the stiffness of the spring to the equivalent spring stiffness at the wheel axle.

6.1 Conclusions

- The standard installation ratio is an incomplete description of the vertical stiffness of the suspension. The use of the ratio leads to an inaccurate description of the vertical stiffness, especially at large angular deflections.

- A different description of the vertical stiffness is derived that is applicable for linear and nonlinear springs and includes a correct translation of the pre-deflection. The description consists of only geometric terms, hence the name **Geometric Equivalent Stiffness**. The geometric terms make the description usable for conceptual design and is extremely accurate.

- The method of Matschinsky is examined for a trailing arm suspension. An extension of this method is made in order to take into account the pre-deflection of the spring. The Matschinsky method is extremely accurate for both linear and nonlinear springs as well as for larger angular deflections. Solving the derivatives $\frac{da}{ds}$ and $\frac{db}{ds}$ using the variables obtained for the geometric equivalent stiffness, results in the same expression as the geometric equivalent stiffness itself.

- An alternative method is developed that describes the vertical stiffness of the trailing arm suspension and relating it to the stiffness of the suspension spring. This alternative method is called the **Modified Installation Ratio** and also includes the correct translation of the pre-deflection. The method is as accurate as the geometric equivalent stiffness and is also applicable for large angular deflections. For conceptual design however it is sometimes easier to use a formulation such as the modified installation ratio instead of the geometric equivalent stiffness. This is because, during development of a vehicle, the equivalent vertical stiffness or wheel rate is determined and then used to compute the actual spring stiffness. The geometric stiffness and the Matschinsky method have an additional term besides their spring ratio that makes the modified installation ratio more favourable for this spring stiffness computation. However, the modified installation ratio is only applicable for linear springs.

- The approach that is used to describe the vertical or equivalent damping is extremely accurate for linear damper characteristics. The approach is not accurate for nonlinear damper characteristics.

- A **Conceptual Suspension Model** is developed that includes a joint connection that replaces the physical trailing arm suspension. The joint consists of the equivalent stiffness and damping as well as the definition of the wheel trajectory. It also takes into account the behaviour of the suspension during braking. Utilizing this total description of the trailing arm suspension results in a considerable reduction in CPU time needed for simulation ($81-86\%$). This reduction also results in a CPU time that consumes only 58 % of the simulation time. The conceptual suspension model is therefore applicable for real-time applications.

- The method to describe the correct behaviour of the suspension during braking proved not to be accurate enough. Proper pitch, vertical force, center of gravity displacements are achieved but the correct description of the anti-effects during braking leaves room for improvement.

6.2 Recommendations

- To properly describe the nonlinear equivalent damping, an alternative method has to be developed. The derivation of the geometric equivalent rate can be used as an useful indication. More research should be done in order to achieve this.

- The brake tests show that the conceptual suspension does not represent the anti-rise accurate enough. It is recommended that more research is done to improve the additional vertical force due to braking. The correct relation between the actual vertical deflection s' of the wheel and the angular deflection θ of the trailing arm is of great importance to accurately describe the anti-dive and anti-rise effects. Thus more research of the implementation of this deflection is recommended.

- This thesis is a start in the development of a full vehicle model that is applicable in a real-time environment. To stay in the two dimensional space, it is recommended that the dynamic effect during acceleration is also investigated before research is done in the three dimensional space. This gives the correct insight in both the brake and acceleration effects.

- It is recommended that the geometric equivalent stiffness derivation and the modified installation ratio is executed for other suspension configurations such as double A-arm suspensions. The assumption of implementing planes for upper and lower suspension arms, as is done by E. Manes and J. Starkey, can be used to obtain a geometric equivalent stiffness in three dimensional space. In this way, the development stays in the URE environment and brings the vehicle model closer to the actual race car.

- The use of lookup tables not only proved to be fast but also practical in use. Hence it is recommended to use look-up tables for future definitions of the wheel trajectories. Of course, the assumption that no suspension compliance is applied is still present. The URE race car however has minimum suspension compliance in order to achieve the desired vehicle handling.

- The conceptual suspension model leaves room for improvement. Certain point masses are used to connect components to each other. A more effective model is accomplished if more bodies can be eliminated.

Bibliography

[1] Matt Davis, *Vehicle Dynamics International*, March 2007.

[2] Wolfgang Matschinsky, *Road vehicle suspensions*, Professional Engineering Publishing ISBN 1 86058 202 8, 2000.

[3] W.F. Milliken and D.L. Milliken, *Race Car Vehicle Dynamics*, Society of Automotive Engineers ISBN 1 56091 526 9, 1995.

[4] Hans B Pacejka, *Tyre and Vehicle dynamics*, Butterworth Heinemann Ltd ISBN 0 7506 5141 5, 2002.

[5] W.F. Milliken and D.L. Milliken, *Chassis Design, principles and analysis*, Society of Automotive Engineers ISBN 1 86058 389 x, 2002.

[6] J.G.Dickison and A.J. Yardley, *Development and Application of a Functional Model to Vehicle Development*, SAE Technical Paper 930835, 1993.

[7] G.J. Choi, Y.M. Yoo, K.P. Lee and Y.S. Yoon, *Vehicle Modeling Methods for Real-time Dynamic Simulation Using Suspension Composite Joints*, Vehicle System Dynamics, vol. 33, no. 2, pp. 303-321, 2000.

[8] A. Eichberger and W. Rulka, *Process Save Reduction by Macro Joint Approach: The Key to Real Time and Efficient Vehicle Simulation*, Vehicle System Dynamics, vol. 41, no. 5, pp. 401-413, 2004.

[9] Enrico Nino Manes and John M. Starley, *Derivation of the Three-Dimensional Installation Ratio for Dual A-Arm Suspensions*, SAE Technical Paper 2004-01-3535.

[10] TESIS DYNAware, *Suspension Analysis Toolbox ve-DYNA*, 2006.

[11] SIMPACK, *Platform Independent Generation of RT- Models*, 2005.

[12] ADAMS, *Conceptual Suspension Module*, 2002.

[13] A van Berkum, *Chassis and Suspension design FSRTE02*, Eindhoven University of Technology, DCT report 2006 023.

[14] dr.ir. I.J.M Besselink, *Lecture notes, Vehicle and Advanced Vehicle Dynamics*, 2005.

Appendix A

Standard Installation Ratio: Implementation in MATLAB

As is mentioned in the report, the different equivalent force methods are compared in MATLAB. First a kinematic test of the reference suspension model is performed and the necessary variables are used to compute the different equivalent stiffness, damping and forces. This appendix discusses the implementation of the different methods and the calculation of certain items that are not available in the literature of the concerning method. An example is the pre-load and damping of the standard installation ratio.

A.1 Pre-load and Equivalent Spring Force of the Standard Installation Ratio

E. Manes and J. Starkey [9] use linearised rates and thus the definition for the equivalent spring rate remains:

$$c_{FA} = i_{Fs}^2 \, c_F \tag{A.1}$$

Using the linearised equivalent spring rate $c_{FA} = F_{FA}/s$, the equivalent spring force F_{FA} can be obtained.

$$F_{FA} = c_{FA} \, s \tag{A.2}$$

To complete the force F_{FA} the equivalent pre-deflection s_0 must be added. Using equation (A.1) and the rate definitions a relation can be obtained for the vertical wheel displacement s as a function of the spring elongation f.

$$\frac{F_{FA0}}{s_0} = I_{Fs}^2 \, \frac{F_{F0}}{f_0} \tag{A.3}$$

$$s_0 = \frac{F_{FA0}}{F_{F0}} \, \frac{f_0}{I_{Fs}^2} \tag{A.4}$$

$$s_0 = \frac{1}{I_{Fs}} \, f_0 \tag{A.5}$$

The final expression for the equivalent pre-deflection s_0 can now be written as a function of the pre-deflection of the actual spring f_0 as is shown in (A.5). The total equivalent spring force then becomes:

$$F_{FA} = c_{FA} \, (s + s_0) \tag{A.6}$$

Little is known about the equivalent damper rate and how the installation ratio is implemented. Even more, the installation ratio of E.Manes and J.Starkey is only applied to obtain the wheel rate. The total vertical force on the wheel equals to the sum of the equivalent spring and damper force.

$$F_z = F_{FA} + F_{DA} \tag{A.7}$$

Nonlinear rates

In the paper of E. Manes and J. Starkey, there is no information of the implementation of a nonlinear spring. Thus to obtain the vertical force, the same method is used as for the implementation of the linear spring. The implementation of damping is the same for linear and nonlinear rates.

Appendix B

Modified Installation Ratio: Limit Analysis of the Modification Factor and Initial Position Computations

B.1 L'Hopital

In simple cases the rule of L'Hopital states that for functions $f(x)$ and $g(x)$, if:

$$\lim_{x \to c} f(x) = \lim_{x \to c} g(x) = 0 \tag{B.1}$$

or

$$\lim_{x \to c} f(x) = \lim_{x \to c} g(x) = \infty \tag{B.2}$$

Then:

$$\lim_{x \to c} \frac{f(x)}{g(x)} = \lim_{x \to c} \frac{f'(x)}{g'(x)} \tag{B.3}$$

As a reminder the Modification Factor 'MF' is given again:

$$MF = \sqrt{\frac{f}{g \tan\theta \cos\theta_s}} \tag{B.4}$$

$$f(\theta) = f \tag{B.5}$$
$$g(\theta) = g \tan\theta \cos\theta_s \tag{B.6}$$

To know wether L'Hopitals rule applies to this second fraction the statements have to be satisfied. Equations (B.5) and (B.6) give the assignments to the numerator and the denominator respectively. First statement (B.1) is applied to $f(\theta)$.

$$f(\theta) = L_s - L_0 = \sqrt{(g\cos\theta - d)^2 + (e - g\sin\theta)^2} - \sqrt{(g\cos\theta_0 - d)^2 + (e - g\sin\theta_0)^2} \tag{B.7}$$

Where L_s (see equation (3.25)) and L_0 are the instantaneous spring length and the natural spring length respectively.

$$\lim_{\theta \to 0} f(\theta) = \sqrt{(g-d)^2 + e^2} - \sqrt{(g-d)^2 + e^2} = 0 \tag{B.8}$$

The same statement has to be satisfied for the function $g(\theta)$.

$$\lim_{\theta \to 0} g(\theta) = \lim_{\theta \to 0} g \tan\theta \cos\theta_s = 0 \tag{B.9}$$

When the angle θ goes to zero the tangent of the angle will also become zero. This causes the whole equation to result in the value zero. One of the statements is now satisfied which means that the rule of

L'Hopital can be applied. To use the rule the derivatives $f'(\theta)$ and $g'(\theta)$ have to be determined starting with $f'(\theta)$. Keeping in mind that L_0 is a constant, the derivation of $f'(\theta)$ is shown below.

$$f'(\theta) = \frac{1}{2}((g\cos\theta - d)^2 + (g\sin\theta + e)^2)^{-\frac{1}{2}}(-2g\sin\theta(g\cos\theta - d) - 2g\cos\theta(e - g\sin\theta))$$
$$f'(\theta) = \frac{-g\sin\theta(g\cos\theta - d) - g\cos\theta(e - g\sin\theta)}{\sqrt{(g\cos\theta - d)^2 + (e - g\sin\theta)^2}} \tag{B.10}$$

From this derivative the limit of $f'(\theta)$ can be calculated.

$$\lim_{\theta\to 0} f'(\theta) = \frac{-ge}{\sqrt{(g-d)^2 + e^2}} \tag{B.11}$$

Next in line is the derivative of $g(\theta)$, $g'(\theta)$. Using the chain rule of differentiation the derivative can be written as follows:

$$g'(\theta) = \frac{g}{\cos^2\theta}\cos\theta_s + g\tan\theta\frac{d(\cos\theta_s)}{d\theta} \tag{B.12}$$

If the limit is calculated for θ going to zero the second term of equation (B.12) will be eliminated because of the tangent. The limit can now be written as:

$$\lim_{\theta\to 0} g'(\theta) = g\cos\theta_s \tag{B.13}$$

The angle θ_s is also dependant of θ and using equation (3.29) results in:

$$\cos\theta_s = \cos(\frac{\pi}{2} - \alpha) = \sin\alpha \tag{B.14}$$
$$\sin\alpha = \sqrt{1 - \cos^2\alpha} \tag{B.15}$$
$$\cos\alpha = \frac{-d^2 - e^2 + g^2 + (g\cos\theta - d)^2 + (e - g\sin\theta)^2}{2g\sqrt{(g\cos\theta - d)^2 + (e - g\sin\theta)}} \tag{B.16}$$

The limit can now be rewritten:

$$\lim_{\theta \to 0} g'(\theta) = g\sqrt{1 - \cos^2 \alpha} \tag{B.17}$$

$$\lim_{\theta \to 0} g'(\theta) = g\sqrt{1 - \{\frac{(2g^2 - 2gd)^2}{4g^2((g-d)^2 + e^2)}\}}$$

$$\lim_{\theta \to 0} g'(\theta) = ge\sqrt{\frac{1}{(g-d)^2 + e^2}}$$

For the sake of convenience the following can be written:

$$x = (g - d)^2 + e^2 \tag{B.18}$$

The limit of the second fraction then becomes:

$$\lim_{\theta \to 0} \frac{f'(\theta)}{g'(\theta)} = \frac{ge}{\sqrt{x}} \frac{1}{ge\sqrt{\frac{1}{x}}} \tag{B.19}$$

$$\lim_{\theta \to 0} \frac{f'(\theta)}{g'(\theta)} = \frac{1}{\sqrt{x}} \frac{1}{\sqrt{\frac{1}{x}}} = x^{-\frac{1}{2}} \, (x^{-1})^{-\frac{1}{2}} = 1 \tag{B.20}$$

The final expression of the limit of the second fraction for θ going to zero becomes:

$$\lim_{\theta \to 0} \sqrt{\frac{f}{g \tan\theta \cos\theta_s}} = 1 \tag{B.21}$$

B.2 Trailing Arm Initial Position

The kinematic test is performed with the trailing arm positioned horizontally. In practice this is not always the case so a closer look has to be taken into the implementation of the trailing arm when it is not orientated horizontally. The modified installation ratio is used as an example. Figure B.1 will give a better insight into what occurs.

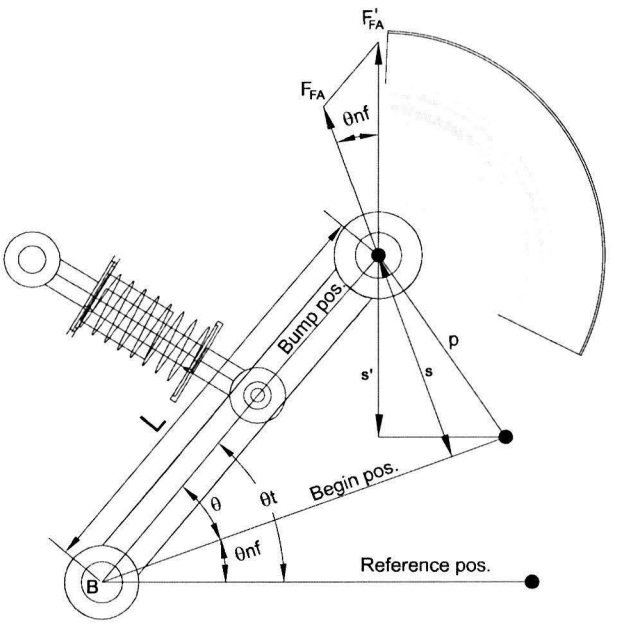

Figure B.1: Situation of a different starting position

To derive the equivalent spring rate c_{FA}, the variables F_{FA} and s were needed. The variable s is assumed to be the vertical displacement and F_z the vertical force. However, this does not apply in the case of a different starting position of the trailing arm. The actual vertical force and displacement are $c_{FA'}$ and s' respectively and the equivalent spring rate is now defined as the quotient of these two. To compute the new equivalent spring rate a relation has to be found for s' which is dependent of the variable s. Using the triangle with the angle θ and the sides L, the straight line distance p emerges. The angles of this triangle are then, θ, $\frac{\pi-\theta}{2}$ and $\frac{\pi-\theta}{2}$. The angle between the sides p and s then becomes $\frac{\pi}{2}-\frac{\pi-\theta}{2}$ and results in $\frac{pi}{2}$. Using the distance p a relation can be formulated for s' and s. Both equations include the distance p which can be isolated in order to merge the two equations. Now a relation can be found for the actual vertical displacement s'.

$$s = p\ \cos\left(\theta/2\right) \tag{B.22}$$

$$s' = p\ \cos\left(\theta/2 + \theta_{nf}\right) \tag{B.23}$$

$$s' = s\ \frac{\cos\left(\theta/2 + \theta_{nf}\right)}{\cos\left(\theta/2\right)} \tag{B.24}$$

Equation B.24 gives the relation for the actual vertical displacement including the term s. The vertical force $F_{FA'}$ can easily be obtained by taking the sum of moments about hinge B.

$$F_{FA'} = F_{FA} \frac{\cos\theta}{\cos\theta_t} \tag{B.25}$$

From here the altered rate $c_{FA'}$ and thus installation ratio is computed again. The installation ratio for the damping and pre-deflection are altered as wel. The only difference now is the angle θ which becomes θ_t.

$$I_{R'} = I_R \sqrt{\frac{\cos\theta}{\cos\theta_t} \frac{\cos(\theta/2)}{(\cos\theta/2 + \theta_{nf})}} \tag{B.26}$$

$$I_{D'} = \frac{g\cos\theta}{L\cos\theta_t} \tag{B.27}$$

The altered modified installation ratio for the spring and damper are given in equation (B.26) and (B.27). A kinematic test is done to check the derivation and the accuracy remains the same. The results are given in figure B.2.

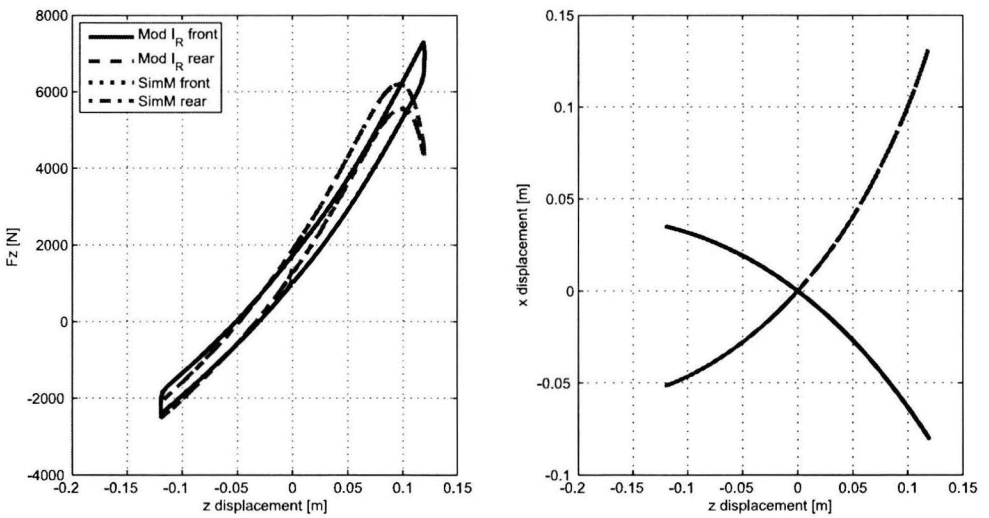

Figure B.2: Vertical force and wheel center location with a different starting position

Appendix C

Matschinsky: Derivative and Velocity Computations

C.1 Implementation in MATLAB

The approach of Matschinsky [2] discusses the derivation of the reduced spring and damper but does not deal with the pre-deflection and the resulting pre-load. Furthermore, there is no example or instruction of how to implement the reduced stiffness and rate into a model.

Reduced Pre-Deflection and Pre-load

As has been explained before, the pre-deflection of the actual spring is different than the one for the reduced spring. The derivation of the equivalent pre-deflection equals the derivation of the geometric equivalent pre-deflection discussed in paragraph 3.1.2. Thus (3.50) is used to obtain the equivalent pre-deflection.

$$s_0 = \int_0^{f_0} \frac{1}{i_F}\, df \tag{C.1}$$

To investigate the reduced spring and damper of Matschinsky, the stiffness and rate have to be implemented MATLAB for comparison. To do so, the variables of equation (2.12) and (2.16) have to calculated or measured.

Reduced spring rate

Starting with the reduced spring. The reduced spring stiffness c_{FA} includes the stiffness of the spring c_F which can be obtained by computing the derivative of the spring function $F_F(f)$ that is given in the suspension model. The spring force F_F , just as the velocities v_a and v_{mz}, can easily be measured within SimMechanics. The velocity v_b however is a variable that has to be obtained indirectly. Appendix C.4 explains the way velocity v_b is obtained. One of the important properties of the Matschinsky derivation of the equivalent stiffness is the equalization of the derivatives of the radii with the velocity ratios.

$$\frac{da}{ds} = \frac{v_a}{v_{mz}} \tag{C.2}$$

$$\frac{db}{ds} = \frac{v_b}{v_{mz}} \tag{C.3}$$

The equalization will not only validate the computed velocity v_b but also validates the reduced spring being implemented correctly. For this purpose the derivatives $\frac{da}{ds}$ and $\frac{db}{ds}$ are computed analytically which can be found in appendix C.2 and C.3 respectively. The computed derivatives and the velocity ratios obtained with the help of SimMechanics are compared with each other. The equalization is plotted in figure C.1.

It is obvious that the results overlap each other which validates the equalization and the criteria mentioned before. The next step is to obtain the vertical force from this reduced spring. Equation (2.9) shows the relation between the reduced spring rate and the vertical force. However, in contrast to the standard installation ratio the force cannot be obtained by simply multiplying the reduced spring rate with the vertical wheel displacement because of the nonlinear nature of c_{FA}. Instead the integral of c_{FA} must be computed to obtain the vertical force.

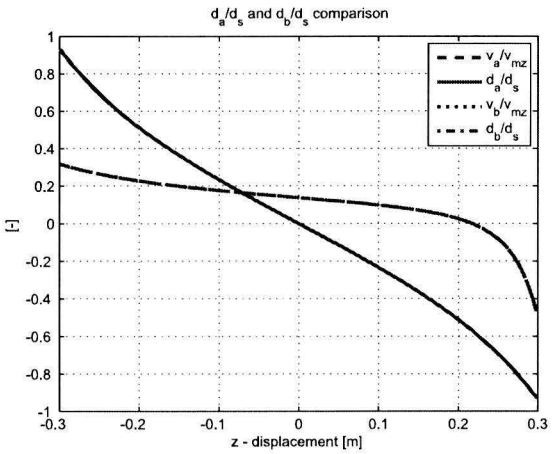

Figure C.1: Proof of equalization of the front suspension

$$c_{FA} = \frac{dF_{FA}}{ds} \tag{C.4}$$

$$F_{FA} = \int_0^{s+s_0} c_{FA}\, ds \tag{C.5}$$

The integral is numerically obtained by applying a 'smoothing spline' fit procedure on the reduced spring rate and integrating this fit within the integration boundaries. This results in the vertical force as function of the vertical wheel displacement plus pre-deflection $s + s_0$. The total vertical force is then:

$$F_z = F_{FA} + F_{DA} \tag{C.6}$$

These data columns are then used for the vertical force comparison within MATLAB.

Reduced damper rate

The damper ratio i_D equals the modified installation ratio for the damper I_{Rd}. This ratio can be obtained by means of the quotient of the radii b and a or by means of the quotient of the velocities v_D and v_{AZ}. Equation (2.15) gives the definition for the reduced damper rate. The variables are instantaneous values in comparison with the ones of the reduced spring rate. The reduced damper force F_{DA} can therefore be obtained by simply multiplying the reduced damper rate with the vertical wheel velocity v_{AZ}.

$$F_{DA} = k_{DA}\, v_{AZ} \tag{C.7}$$

The curve of the damping of the front suspension is shown in figure C.2.

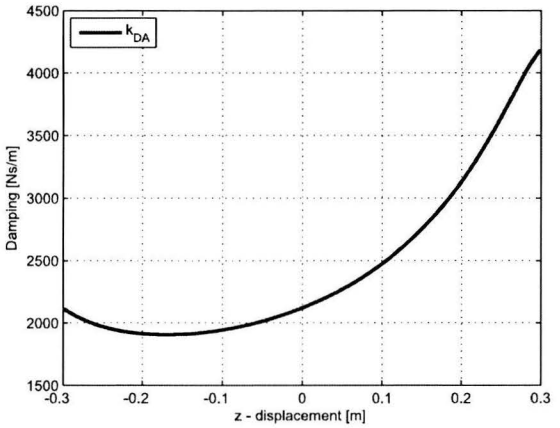

Figure C.2: Reduced damping

C.2 Derivative $\frac{da}{ds}$

The vertical displacement of the wheel s and radius a can be written as is shown below.

$$s = L \sin\theta \tag{C.8}$$
$$a = L \cos\theta \tag{C.9}$$

Assuming that the trailing arm is rigid and thus L is constant:

$$\frac{da}{ds} = \frac{da/d\theta}{ds/d\theta}$$
$$\frac{da}{ds} = \frac{-L \sin\theta}{L \cos\theta} = -\tan\theta \tag{C.10}$$

C.3 Derivative $\frac{db}{ds}$

The derivation of db/ds is more difficult because the dimension 'b' is dependent on θ_s. The angle θ_s is a calculated value. θ_s is a function of several variables. First, the variable b can be written as follows:

$$b = g \cos\theta_s \tag{C.11}$$

The derivative db/ds can be written as:

$$\frac{db}{ds} = \frac{db}{d\theta}\frac{d\theta}{ds} \tag{C.12}$$

This action gives the opportunity to compute the last fraction which is the derivative $d\theta/ds$.

$$\frac{ds}{d\theta} = L\cos\theta \tag{C.13}$$

$$\frac{d\theta}{ds} = \frac{1}{L\cos\theta} \tag{C.14}$$

The first fraction contains the variable b which is dependent on θ_s. To compute the derivative a relation must be found between θ and θ_s.

$$\frac{db}{d\theta} = \frac{db}{d\theta_s}\frac{d\theta_s}{d\theta} \tag{C.15}$$

$$\frac{db}{d\theta_s} = -g\sin\theta_s \tag{C.16}$$

The derivative $d\theta_s/d\theta$ is discussed in paragraph 3.1.1. Substituting (3.44) and (C.16) into (C.15) results in:

$$\frac{db}{d\theta} = \frac{db}{d\theta_s}\frac{d\theta_s}{d\theta} = \frac{-g\sin\theta_s}{\sin\alpha}\frac{(x+d^2+e^2-g^2)y}{4gx\sqrt{x}} \tag{C.17}$$

Reminding equation (C.12) and (C.14) results in the final relation for $\frac{db}{ds}$.

$$\frac{db}{ds} = \frac{db}{d\theta}\frac{d\theta}{ds} = -\frac{g\sin\theta_s}{L\cos\theta\sin\alpha}\frac{(x+d^2+e^2-g^2)y}{4gx\sqrt{x}} \tag{C.18}$$

C.4 Obtaining velocity v_b

The velocity v_b cannot be measured directly. However, the velocity can be computed with the help of SimMechanics. SimMechanics can measure the velocity components in x and z direction of the mounting point of the spring on the trailing arm. The velocity at this mounting point that is positioned perpendicular with respect to the trailing arm is called v_B which can be seen in figure C.3. The velocity components measured in SimMechanics used to compute v_B are called v_{Bx} and v_{Bz} (not shown in figure C.3). The velocity v_B can be derived using the Pythagoras theorem.

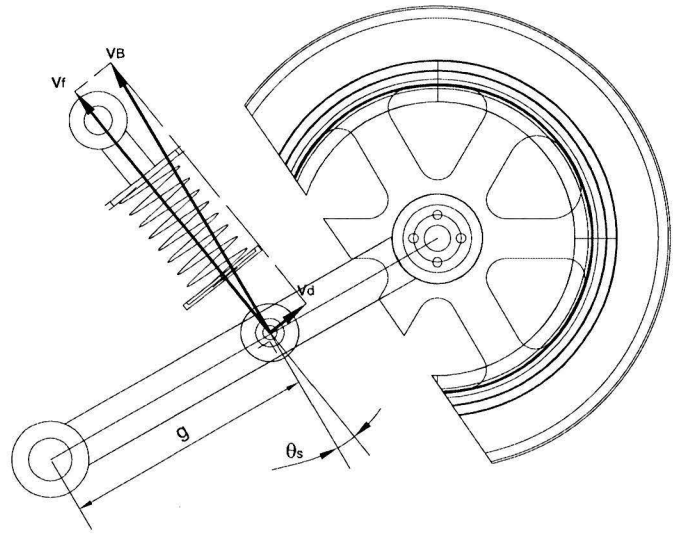

Figure C.3: Velocity v_B

$$v_B = \sqrt{v_{Bx}^2 + v_{Bz}^2} \tag{C.19}$$

The velocity v_B can now be split in a component parallel and a component perpendicular to the axis of the spring. These components are the spring velocity v_f and the velocity v_d respectively. Using simple trigonometry a relation can be found for v_d.

$$v_d = v_B \sin\theta_s \tag{C.20}$$

The velocity vector v_d, length l_s and the aligned distance between the top spring mounting point and v_d form a triangle as can be seen in figure C.4. The lengths l_t and l_v are defined as the lengths from the velocity vector v_b to the lower and upper mounting point of the spring.

$$l_t = g \sin\theta_s \tag{C.21}$$
$$l_v = l_s - l_t \tag{C.22}$$

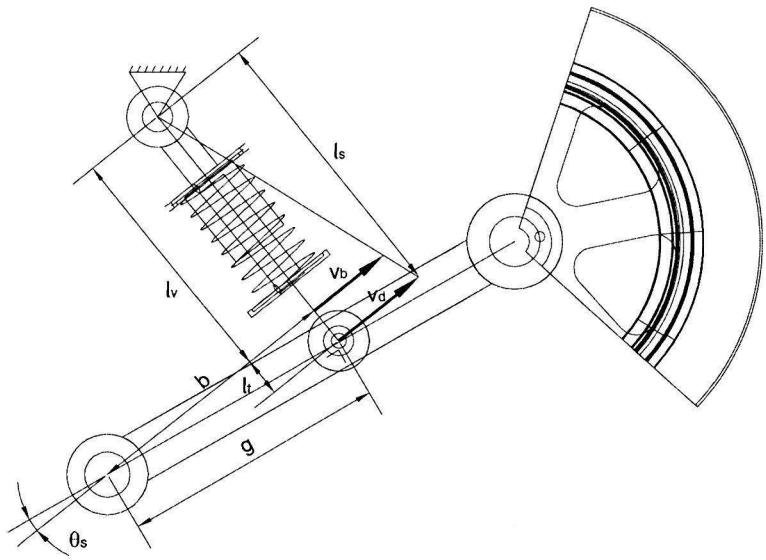

Figure C.4: Velocity v_b

Using the theorem of uniform triangles the final expression can be given for the velocity v_b.

$$v_b = v_d \frac{l_v}{l_s} \tag{C.23}$$

Appendix D

Design Forces and Dimensions of the Reference Suspension Model

D.1 Reference Suspension Model

This appendix describes the process of developing the two dimensional reference suspension model. This includes the derivation of the design forces, such as nominal loads and vertical forces due to the load transfer during braking, defining the dimensions of the suspension and computing the values for the spring stiffness and damping in order to create the suspension model.

The vehicle model contains a trailing arm suspension with a spring and damper combination. The three dimensional graphical representation of the trailing arm suspension being used in this thesis is shown in figure D.1.

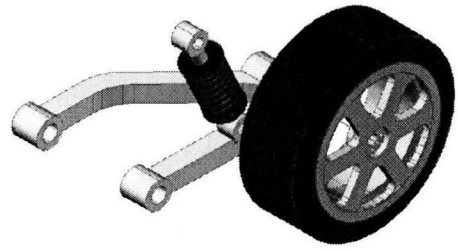

Figure D.1: Graphical representation of the suspension model

The vehicle with the suspension model is based on the dimensions and mass properties of the formula student car FSRTE02 [13]. The formula student car has a double A-arm suspension so the suspension dimensions can not be inherited by the trailing arm suspension. In addition, the spring system is different. Dimensions that the reference suspension does inherited from the race car are the wheelbase, height of the center of gravity, etc. The dynamics of the vehicle depend on these dimensions. In order to design the dimensions of the suspension, stiffness of the spring, etc design forces as nominal loads and brake forces have to be obtained.

D.2 Design Forces

The suspension of the model can have various configurations dependent on the criteria that have been determined for the vehicle. The schematic diagram of the vehicle can be seen in figure D.2.

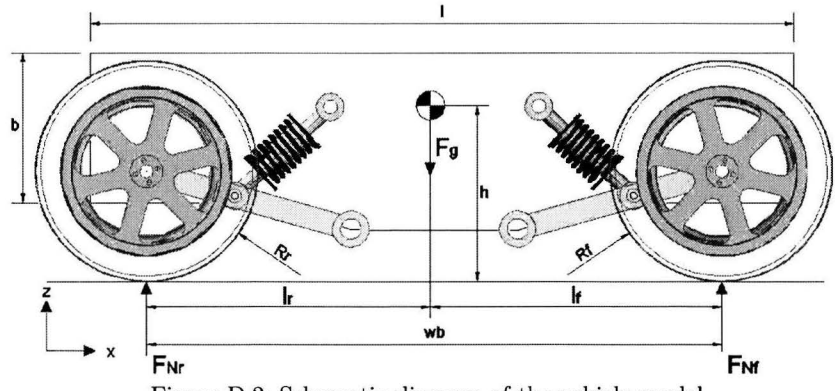

Figure D.2: Schematic diagram of the vehicle model

The nominal vertical forces at the tyre contact patch are simple to calculate. However during braking a load transfer will occur causing an increase or decrease in vertical force. The vertical forces on the tyre contact patch must be obtained followed by the brake forces at the front and rear tyres.

During a brake situation the front of the vehicle will tend to dive and the rear will tend to rise. The suspension can be engineered is such a way that these effects will be reduced or even eliminated. Influencing these effects can be realised by using the anti-dive and anti-rise relations. In this thesis the vehicle model will have a brake system that is based on the deceleration a_x, the resulting brake forces F_b and the brake force distribution p. The brake force distribution divides the applied brake torque and thus force to the brake system into separate amounts for the front and rear axle. The forces acting on the front suspension during braking and the suspension dimensions are shown in figure D.3.

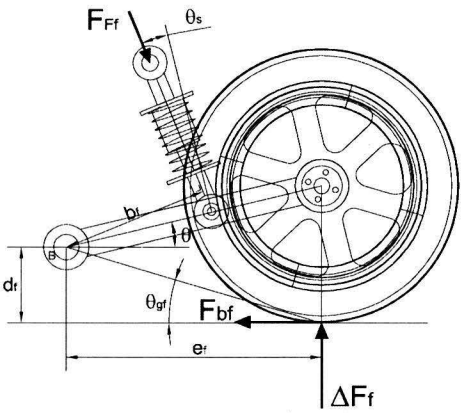

Figure D.3: Anti-dive and anti-rise variables of the front suspension during braking

The amount of anti-dive of the front suspension is set to 70% which results in a value for $\tan\theta_{gf}$. This leaves an engineering choice for the length of e_f and d_f which leads to the dimensions of the suspension as trailing arm length and the position of the hinge. The same methodology can be applied for the amount of anti-rise for the rear suspension. The amount of anti-rise is set to 30%. The lectures of [14] are used to obtain the brake forces and anti-dive and anti-rise variables. The final design values that have to be obtained are the spring and damper rates of the suspension and thus the suspension springs and dampers.

The dynamics of the vehicle and thus the suspension is based on the demands of the vehicle being developed. Does the vehicle have to be comfortable, is improved handling preferable or is a compromise desirable. This is partly dependent on the maximum frequencies the sprung and unsprung masses can take in order to sustain the resulting vibrations. Of course, the masses can be designed to sustain desired frequencies. The vibrations are categorized in the so called 'vehicle ride'. Vehicle ride has a primary part and a secondary part according to [5]. Primary ride is defined as 'the low frequency vibration of the sprung mass as a rigid body'. The secondary ride involves the unsprung mass vibration and is defined as 'Hop, the vertical oscillatory motion of the unsprung mass between the road surface and the sprung mass'. The frequency of the hop modes is well above that of the primary mode so these modes do not interfere each other. In addition, the road surface on which the models will be tested is assumed to be ideal flat. With these points in mind the rate of the suspension will be obtained by using the primary ride only. The low frequency of the primary ride, or chassis natural frequency ω_c, can rise up to approximately 5 [Hz] for racing cars [5]. The URE team uses a 2,5 [Hz] natural frequency from which the wheel rate of the suspension can be computed. Literature of [5] is used to obtain the stiffness and damping of the suspension spring and damper.

The design forces are now calculated and suspension dimensions are chosen accordingly. Numerical values of the these forces and dimensions are given in the table below.

Vehicle dimensions	[m]	Suspension dynamics		Suspension dimensions	[m]
wb	1,550	ζ	0,5 [-]	e_f	0,400
h	0,317	ω_c	2,5 [Hz]	e_r	0,300
l	1,800			d_f	0,076
b	0,350	m_{cf}	135,6 [kg]	d_r	0,076
l_f	0,837	m_{cr}	159,4 [kg]		
l_r	0,713	m_{wf}	7,05 [kg]		
R_f	0,257	m_{wr}	7,95 [kg]	Design forces	[N]
R_r	0,275				
a_x	14,7 $[m/s^2]$	c_{Ff}	87015 [N/m]	F_{Nf}	1399
μ_{longf}	1,46 [-]	c_{Fr}	90310 [N/m]	F_{Nr}	1642
μ_{longr}	1,88 [-]	k_{Df}	5540 [Ns/m]	F_{bf}	3238
p	0,75 [-]	k_{Dr}	5750 [Ns/m]	F_{br}	1271

Figure D.4: Model dimensions, design parameters and forces

D.3 Nonlinear spring and damper characteristics

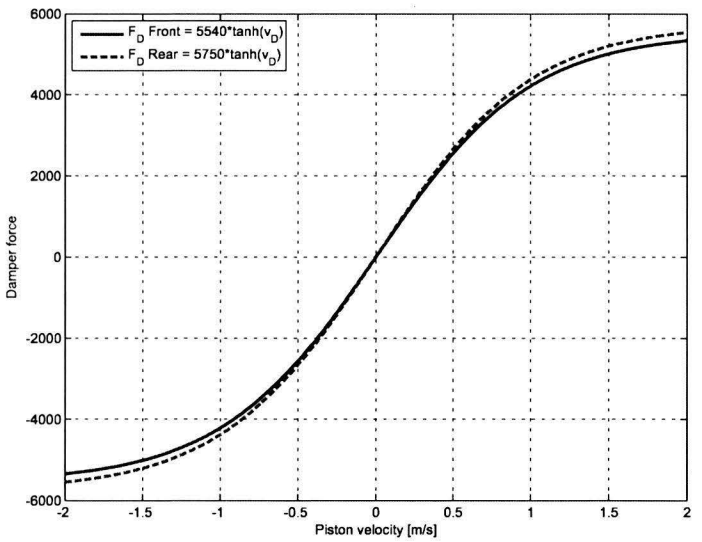

Figure D.5: Nonlinear damper characteristic of the front and rear damper

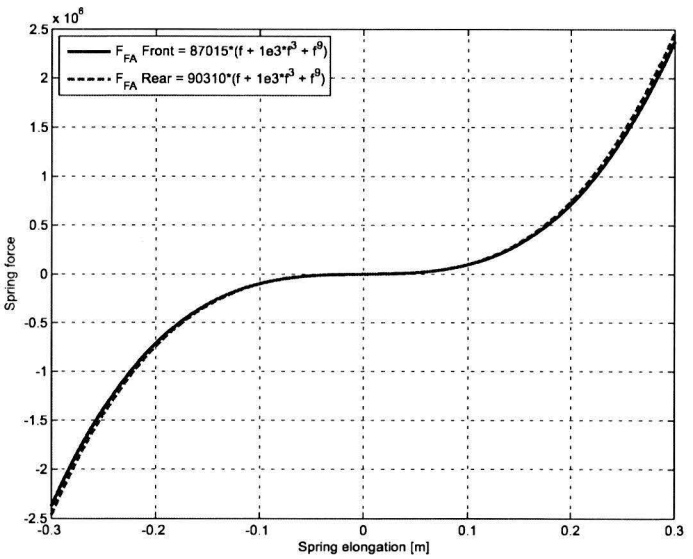

Figure D.6: Nonlinear stiffness characteristic of the front and rear spring